

UNIVERSITY OF TEXAS AT ARLINGTON

MASTERS THESIS

**Sensitivity Study for Low Mass
Dark Matter Search at DUNE**

Author:
Garrett BROWN

Supervisor:
Dr. Jaehoon YU

*A thesis submitted in fulfillment of the requirements
for the degree of Masters of Science in Physics*

in the

High Energy Physics Group
Department of Physics

April 4, 2018

Declaration of Authorship

I, Garrett BROWN, declare that this thesis titled, “Sensitivity Study for Low Mass Dark Matter Search at DUNE” and the work presented in it are my own. I confirm that:

- This work was done wholly or mainly while in candidature for a research degree at this University.
- Where any part of this thesis has previously been submitted for a degree or any other qualification at this University or any other institution, this has been clearly stated.
- Where I have consulted the published work of others, this is always clearly attributed.
- Where I have quoted from the work of others, the source is always given. With the exception of such quotations, this thesis is entirely my own work.
- I have acknowledged all main sources of help.
- Where the thesis is based on work done by myself jointly with others, I have made clear exactly what was done by others and what I have contributed myself.

Signed:

Date:

“A physicist is like a painter, the paint and brush are mathematics and computers and that ugly thing over there I have to figure out how to paint is the universe.”

UNIVERSITY OF TEXAS AT ARLINGTON

Abstract

Dr. Jaehoon Yu
Department of Physics

Masters of Science in Physics

Sensitivity Study for Low Mass Dark Matter Search at DUNE

by Garrett BROWN

Many anomalies in the predictions of mass and gravity at the galactic scale have been attributed to an elusive form of matter we refer to as dark matter. The excessive rotational velocity of galaxies and gravitational lensing observed in the cosmos have not found any explanation within the standard model of physics. However, dark matter itself remains undetected as it seems to only interact with gravity. If it does interact with other forces, it has a minuscule cross section similarly to the neutrino particle. Many emerging theories hope to explain the mechanisms of production and interaction of dark matter and many future experiments hope to detect it. It is thought that the detection of dark matter will be more likely by producing boosted dark matter with the use of high energy particle accelerators, and since dark matter is also thought to interact similarly to the neutrino, the use of a neutrino detector also proves to be a good choice. These are all components of the Deep Underground Neutrino Experiment (DUNE) at Fermilab. This paper explores the possibility of detection in the low mass range of light dark matter at DUNE using electron elastic scatter events in the Near detector. We use computer simulations of dark matter and neutrinos produced in the experiment and their signals in the detector to set 90% confidence limits over the light dark matter parameter space.

Acknowledgements

There are many people who helped make this paper possible. My friends who provided me entertainment during times of much needed breaks and support during times of distress and hardship. My friend Chris who throughout this endeavor provided undying encouragement and motivation. My parents who provided guidance and motivation in times of need. My professors of the university who provided a solid foundation for the math and physics required in the understanding of this research and the guidance needed for my success in graduate school.

I am thankful to Jaehoon Yu who helped me enroll in the University of Texas at Arlington and offered to be my advisor. He helped me get involved with high energy physics at Fermilab and introduced me to many collaborators in the DUNE project. His advice throughout this research has been vital and I thank him for remaining patient with me during times when classes and life proved overwhelming.

I am also thankful to Animesh Chatterjae who helped get this analysis started and get me up to speed.

Finally, much of the technical difficulties we had with the Fermilab computing systems would have deadlocked our progress without the knowledge and support of the amazing faculty of the Fermilab National Laboratory. Thanks very much.

Contents

Declaration of Authorship	i
Abstract	iii
Acknowledgements	iv
1 Introduction	1
1.1 Physics Motivation	1
1.2 The DUNE Experiment	5
2 Dark Matter Theory	11
2.1 Theoretical Background	11
2.2 Light Dark Matter Model	12
2.3 Production	14
2.4 Detection	15
3 Experimental Setup	17
3.1 Software Simulation	17
3.1.1 Fermilab Computing Grid	18
3.1.2 MadGraph5	20
3.1.3 G4LBNE	22
3.1.4 DuneDM Detector Signal	23
4 Simulation Results	30
4.1 Observations	39
5 Sensitivity	41
5.1 Calculation	41
5.2 Results	43
6 Conclusion	45
A Dark Matter Job Management Script	47
A.1 Usage	50

List of Figures

1.1	The rotation curve of M33. The points are the data measured from M33, the continuous line is the best fit model, the dot-dashed line is the dark matter contribution in the model, the short-dashed line is the stellar disc contribution, and the long-dashed line is the gas contribution. From Ref. [1]	2
1.2	A 3-D reconstruction of dark matter structure in the COSMOS observation field. Slices show the evolution of structure in time where further away slices are further in the past. From Ref. [2]	4
1.3	A density map of visible matter (left) and Dark matter (right) in the COSMOS observation field. From Ref. [2]	5
1.4	A density map of dark matter in a simulated volume of the universe. Two versions of the simulation, TNG100 and TNG300, are shown with closeups of galaxy formation and interstellar dark matter halos. From Ref. [3]	6
1.5	An illustration of the proposed LBNF neutrino beamline. From Ref. [4]	7
1.6	An illustration of the neutrino production mechanism (Note: three horns are used in LBNF rather than two). From Ref. [4] .	9
1.7	An illustration of the Fine Grained Tracking system proposed for DUNE. From Ref. [5]	10
2.1	Dark matter direct production Feynman diagram. From Ref. [6]	14
2.2	Dark matter neutral current elastic scattering from electrons. From Ref. [7]	16
3.1	Block diagram of the simulation showing the steps needed to reach the final result.	28
3.2	Computing statistics of a batch of jobs on cluster machines reported by Fermilab's FIFEMon.	29
3.3	A rendering of the latest G4LBNE simulation models to date. The decay pipe and other containment volumes are not shown here.	29
4.1	Dark matter and Electron Neutrino distributions at the stages of the simulation. Low mass dark matter $m_\chi = 50(\text{MeV})$ with Low Kinetic Mixing $\kappa = 10^{-4}$	31
4.2	Electron signal from Dark matter and Electron Neutrinos. Low mass dark matter $m_\chi = 50(\text{MeV})$ with Low Kinetic Mixing $\kappa = 10^{-4}$	32

4.3	Dark matter and Electron Neutrino distributions at the stages of the simulation. Low mass dark matter $m_\chi = 50(\text{MeV})$ with High Kinetic Mixing $\kappa = 10^{-2}$	33
4.4	Electron signal from Dark matter and Electron Neutrinos. Low mass dark matter $m_\chi = 50(\text{MeV})$ with High Kinetic Mixing $\kappa = 10^{-2}$	34
4.5	Dark matter and Electron Neutrino distributions at the stages of the simulation. High mass dark matter $m_\chi = 3(\text{GeV})$ with Low Kinetic Mixing $\kappa = 10^{-4}$	35
4.6	Electron signal from Dark matter and Electron Neutrinos. High mass dark matter $m_\chi = 3(\text{GeV})$ with Low Kinetic Mixing $\kappa = 10^{-4}$	36
4.7	Dark matter and Electron Neutrino distributions at the stages of the simulation. High mass dark matter $m_\chi = 3(\text{GeV})$ with High Kinetic Mixing $\kappa = 10^{-2}$	37
4.8	Electron signal from Dark matter and Electron Neutrinos. High mass dark matter $m_\chi = 3(\text{GeV})$ with High Kinetic Mixing $\kappa = 10^{-2}$	38
5.1	The 90% confidence level of (Y vs m_χ)	43
5.2	The 90% confidence level of (Y vs m_χ) imposed on other analyses. From Ref. [7].	44

List of Tables

List of Abbreviations

DUNE	Deep Underground Neutrino Experiment
LBNF	Long Baseline Neutrino Facility
FGT	Fine Grained Tracker
ECAL	Electromagnetic Calorimeters
CC	Charged Current
NC	Neutral Current
LArTPC	Liquid Argon Time Projection Chamber
LO	Leading Order
NLO	Next to Leading Order
QCD	Quantum Chromodynamics

Physical Constants

Speed of Light	$c_0 = 2.997\,924\,58 \times 10^8 \text{ m s}^{-1}$ (exact)
Fine-Structure Constant	$\alpha_e = 1/137.035999139(31)$ (exact)
Mass of electron	$m_e = 510.9989$ (KeV/c ²) (approx)
Archimedes' constant (Pi)	$\pi = 3.1415926535897\dots$ (exact)

List of Symbols

V	Light dark matter mediator	
χ	Light dark matter particle	
$\bar{\chi}$	Light dark matter antiparticle	
p	Proton particle	
ν_e	Electron Neutrino particle	
m_V	Light dark matter mediator mass	(GeV)
m_χ	Light dark matter mass	(GeV)
q_B	Light dark matter mediator baryon number	
q_χ	Light dark matter charge (1)	
κ	Light dark matter kinetic mixing	
α	Light dark matter $U(1)'$ gauge coupling	
α_e	The fine-structure constant	
γ	The gamma matrices	
E	Particle energy	(GeV)
θ	Particle azimuthal angle with beam direction	(rad)
σ	Production or scattering cross section	(cm ²)
Z	Density of nucleons or electrons	(cm ⁻³)
ϵ_{eff}	Detector efficiency	
χ^2	The reduced chi-squared statistic	

Dedicated to my parents.

Chapter 1

Introduction

1.1 Physics Motivation

The idea for dark matter first began nearly a century ago after observations of the rotational velocities of galaxies in relation to their mass failed to satisfy basic kinematics. Centripetal acceleration did not agree with the gravitational acceleration. In 1933, Astronomer Fritz Zwicky was the first to obtain accurate evidence of this by applying the virial theorem to velocity and mass measurements of the Coma Cluster, and he concluded that the cluster required 400 times more mass than was visually observable for its shape to be maintained [8]. This estimation would be later lowered as more accurate measurements and changes to the Hubble constant were made, but the problem still remains. One might think one simple explanation could be that there is indeed more mass inside the galaxy except that it is shrouded by dust or simply hidden in the core, but not only is the rotational velocity faster than normal, the function of rotational velocity with respect to radius from the center, known the galaxy's rotation curve, also does not match expected predictions. When a mass distribution model incorporating a dark matter mass distribution is added to the system, the data finally aligns with the model. One example of this fit was done in 1999 by Edvige Corbelli and Paolo Salucci of the nearby M33 galaxy [1]. Rotational velocity was measured out to a galactocentric distance of 16kpc and the radial distribution of stars and

gas were used to fit a rotation curve that incorporates dark matter. Fig.(1.1) shows the M33 rotation curve as points fitted to the best-fitting model which is plotted as a continuous line. The contributions to the rotational velocity from each component of matter in the galaxy are also presented as dashed lines. The dot-dashed line, short-dashed line, and long-dashed line correspond to the contributions of the dark matter halo contained in the galaxy, the stellar disc, and the interstellar gases respectively. Using this fit, The density profile of dark matter is predicted and shows a radial decrease as $R^{-1.3}$ which matches theoretical predictions for cold dark matter hierarchical clustering models [1].

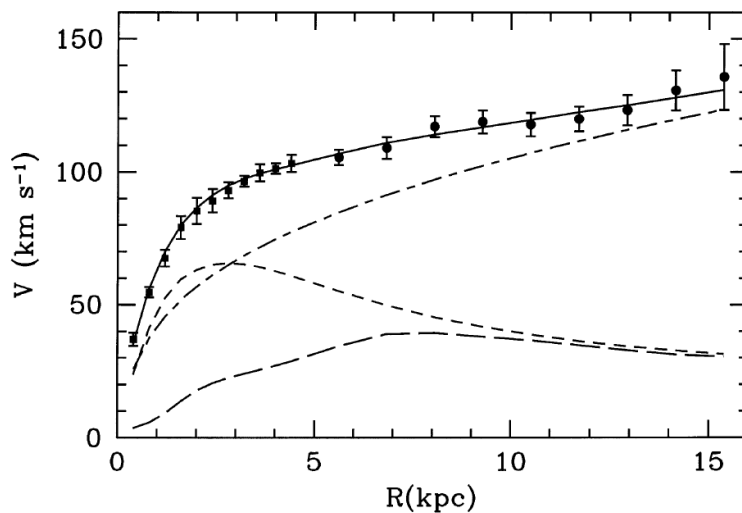


FIGURE 1.1: The rotation curve of M33. The points are the data measured from M33, the continuous line is the best fit model, the dot-dashed line is the dark matter contribution in the model, the short-dashed line is the stellar disc contribution, and the long-dashed line is the gas contribution. From Ref. [1]

After its proposal in the 1930s, though, physicists were still skeptical of a new unseen particle. Theories of light absorption in dust causing inaccurate measurements or even theories of Modified Newtonian dynamics (MOND) were proposed. It wouldn't be until 30 years later that it was taken seriously when Vera Rubin and Kent Ford obtained far more accurate data from

the M31 Galaxy aka. the Andromeda Galaxy using the new DTM image-tube spectrograph [9]. Since then, many new observations confirming their observations and supporting dark matter's existence have been made. One very recent one by the LIGO detector and SWOPE telescope recorded measurements of gravity waves and photons emitted from a binary neutron star merging. The Shapiro delay between the gravity waves and photons/neutrinos arrival further suggests existence of dark matter and discredits several (MOND) theories [10]. Gravitational lensing is another phenomena that has been observed and has been used extensively in mapping the densities of dark matter in space [2]. One collaboration effort using it now is the Cosmic Evolution Survey (COSMOS) and it is surveying a field of sky roughly "8 times the size of the moon" [2] with various telescopes including the Hubble Space Telescope, Europe's Very Large Telescope, Japan's Subaru Telescope, the U.S. Very Large Array radio telescope, and the XMM-Newton X-ray observatory. Combining the data and using distortions in the images between each telescope, the gravitational lensing can be calculated and 3D dark matter distributions can be reconstructed. Fig.(1.2) and Fig.(1.3) show a 3D and 2D density map of dark matter in the COSMOS observation field. Because photons used to reconstruct dark matter at further distances have been travelling for longer time, the reconstructed dark matter structures at further distances show us what structure in the past looked like and provide groundbreaking insight into how dark matter structures have evolved since the big bang.

These observations have also been in the process of being duplicated via computer simulation. MIT's IllustrisTNG project is currently the largest and most realistic hydrodynamical simulation capable of simulating the evolution of clusters of galaxies and dark matter [11]. Such simulations are being analyzed and compared against real observations to test the dark matter

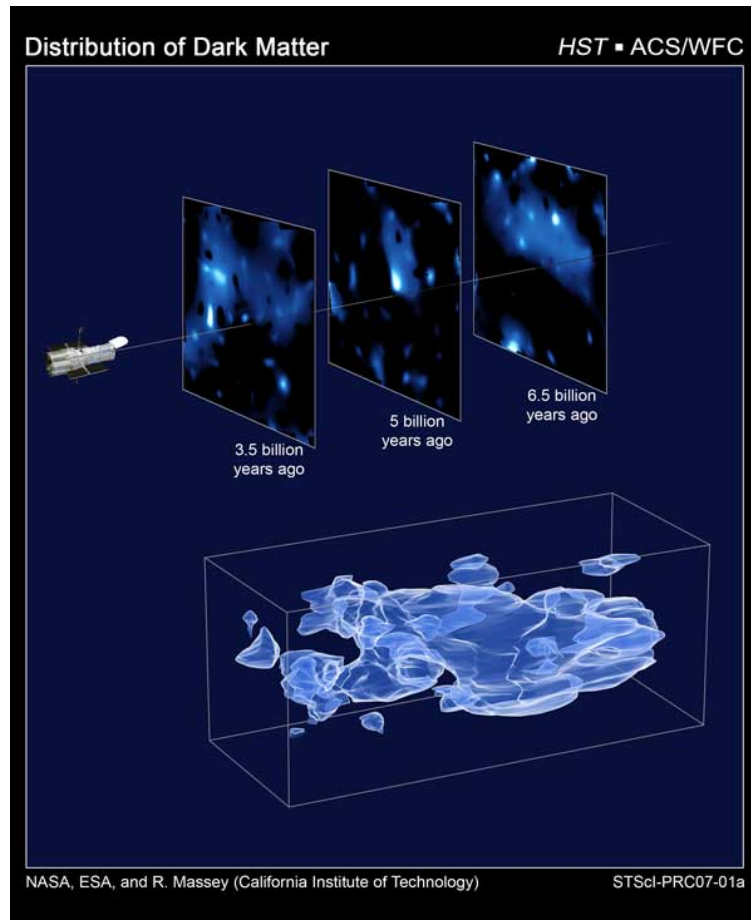


FIGURE 1.2: A 3-D reconstruction of dark matter structure in the COSMOS observation field. Slices show the evolution of structure in time where further away slices are further in the past. From Ref. [2]

models implemented in the simulation, and they currently show striking resemblance to current observations. They further show that formations of galaxies and clusters rely heavily on dark matter. Fig.(1.4) shows a rendering from the Illustris TNG100 and TNG300 simulation of dark matter structure in the universe.

Despite the overwhelming evidence for dark matter. The particle itself has not been detected yet and its processes are unknown. There are many aspects of it that have been predicted which will be elaborated on later, but in order to definitively learn about it, a detection must be made. The DUNE experiment has some prospect for this.

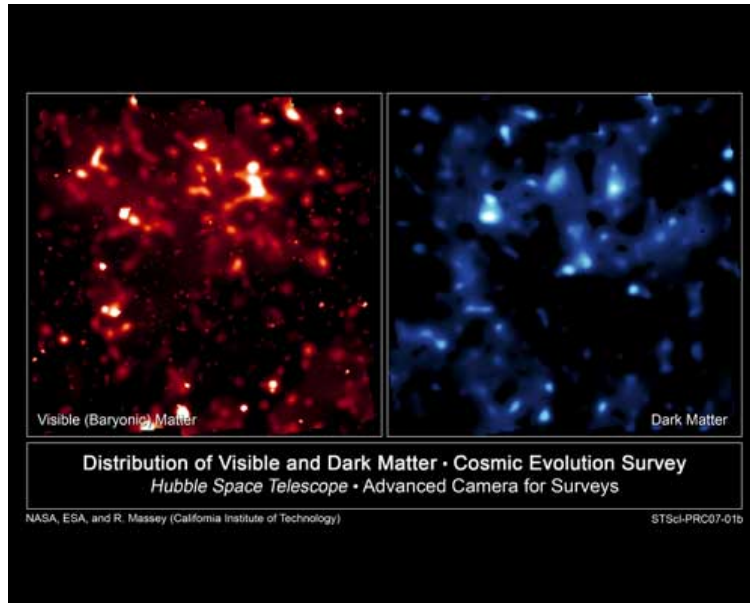


FIGURE 1.3: A density map of visible matter (left) and Dark matter (right) in the COSMOS observation field. From Ref. [2]

1.2 The DUNE Experiment

The DUNE experiment is an international collaboration effort towards the next generation long-baseline neutrino experiment [12]. Thanks to funding from the U.S. Department of Energy, expansions to the underground infrastructure at the Sanford Underground Research Facility in South Dakota and creation of a megawatt neutrino facility at Fermilab are possible, so it has been decided to take place here in the U.S. at Fermilab. Funding from many other countries and organizations including CERN will also contribute to DUNE. With the PIP-II accelerator upgrade, it is expected to drive the neutrino beamline with a power of up to 1.2 MW by 2026 and another upgrade producing up to 2.4 MW by 2030 [12].

The purpose of the deep underground neutrino experiment is, as its name implies, to study neutrinos. In the past years, many new discoveries related to neutrinos has suggested new physics beyond the Standard Model. One of such is neutrino flavor oscillation, which allows neutrinos to transform their flavor while they propagate through space. This phenomenon

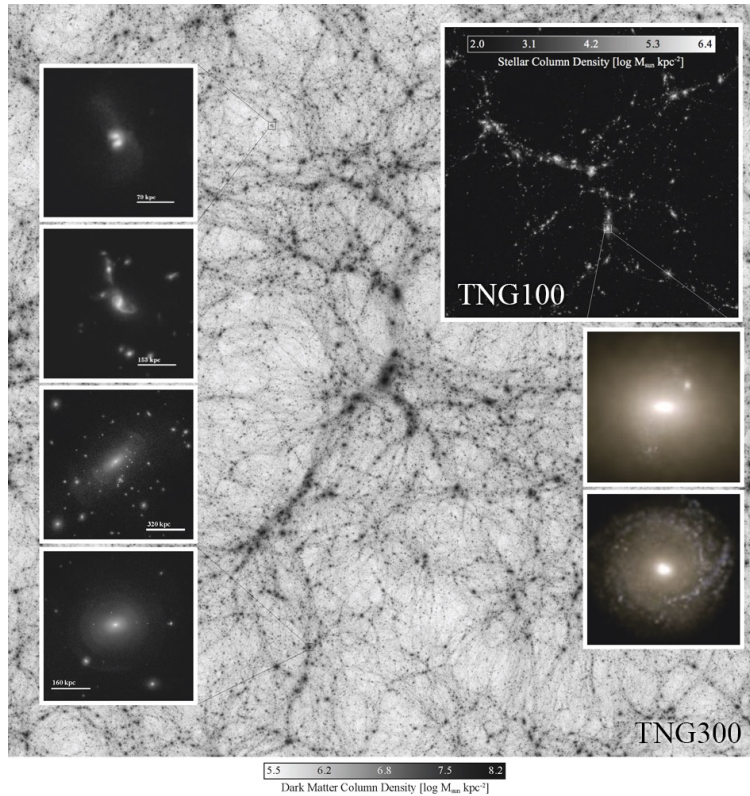


FIGURE 1.4: A density map of dark matter in a simulated volume of the universe. Two versions of the simulation, TNG100 and TNG300, are shown with closeups of galaxy formation and interstellar dark matter halos. From Ref. [3]

is described by quantum-mechanical mixing of their three mass eigenstates and their flavor eigenstates and is parameterized in the Pontecorvo-Maki-Nakagawa-Sakata matrix [12]. The Pontecorvo-Maki-Nakagawa-Sakata matrix also predicts a charge-parity (CP) violating phase in neutrinos. Currently, experimental data agrees with this three-neutrino paradigm of the three neutrino-flavor states but with some anomalies. DUNE's objective is to carry out a comprehensive investigation of neutrino physics by testing the neutrino oscillation predictions, testing for CP violations in the lepton sector, and determining neutrino mass hierarchy with great precision. By measuring the parameters that govern $\nu_\mu \rightarrow \nu_e$ and $\bar{\nu}_\mu \rightarrow \bar{\nu}_e$ oscillations, the charge-parity violating phase angle δ_{CP} can be determined. If δ_{CP} is anything but zero or π , CP violation in the leptonic sector would be confirmed. Such a discovery could explain the matter-antimatter asymmetry in the universe

[12]. Measuring neutrino mass hierarchy, $\Delta m_{31}^2 \equiv m_3^2 - m_1^2$, and other properties of neutrino mixings and comparing them with the quark sector may help understand other fundamental underlying symmetries of the universe. It is also thought that DUNE may be able to detect certain proton decay modes, such as $p \rightarrow K^+ \bar{\nu}$. A discovery of this would allow progress towards a Grand Unification of forces. DUNE may also be able to measure neutrino flux and gather data from a core-collapse supernova in our galaxy if one of such were to occur. Information from these measurements could provide insight into the dynamics of supernovae and neutrinos physics involved in them.

For DUNE to achieve its goals, it will utilize the LBNF (Long Baseline Neutrino Facility) which comprises the entire beamline of the experiment. The LBNF beamline is designed after another successful neutrino beamline known as NuMI which was used for the NOvA experiment [12]. From start to finish, it includes the Fermilab proton accelerator, the proton target hall; focusing horns; decay pipe; and absorber, Near Detector, and, 800 miles further downstream, the far detector. All components will be located on-site at Fermilab except for the far detector, which is located at the Sanford Underground Research Facility. Both detectors are located deep underground in order to minimize background from cosmic radiation. Fig.(1.5) provides an illustration of the proposed beamline.

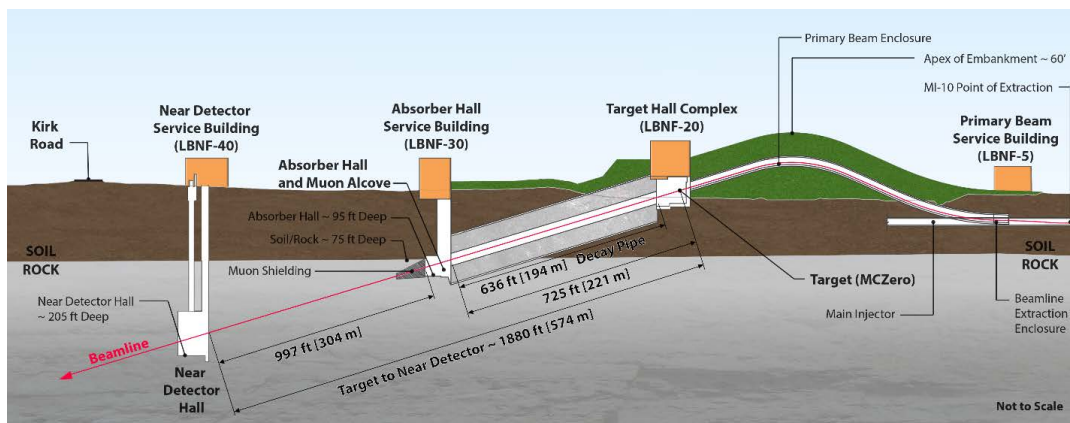


FIGURE 1.5: An illustration of the proposed LBNF neutrino beamline. From Ref. [4]

The beamline starts with protons from Fermilab's Main Injector synchrotron which will be extracted using a single-turn extraction method with a nominal energy of 60 to 120 GeV and then transported to the LBNF Target Hall [4]. The beam energy variation will allow optimization of the neutrino flux spectrum and deduction of systematics in the neutrino beam production. The proton beam next reaches the target hall, focusing horns, decay pipe, and absorber which all compose of the mechanism used for neutrino production and, theoretically as this paper will explore, dark matter production. As the protons enter the Target Hall, they will strike a dense and narrow target consisting of graphite, inelastically scattering to produce a shower of mostly pions and kaons. The charged pions and kaons will then travel through a series of three magnetic focusing horns where the Lorentz force law will either focus or disperse them depending on the direction of current in the horns. For our purposes, the dark matter has no charge so it is unaffected by the horns. By changing the direction of current in the horns, neutrinos or anti-neutrinos can be separated; for neutrinos it will focus positively charged kaons and pions $\pi^+ \rightarrow \mu^+ + \nu_\mu$ or $\pi^+ \rightarrow e^+ + \nu_e$, and negatively charged kaons and pions will be focused for anti-neutrino production $\pi^- \rightarrow \mu^- + \bar{\nu}_\mu$ or $\pi^- \rightarrow e^- + \bar{\nu}_e$. This process of decay into neutrinos and other daughter particles occurs in the decay pipe. All particles except for neutrinos and dark matter are then stopped by the absorber, allowing neutrinos and dark matter to reach the 'Near Detector' without interference of the other particles. Fig.(1.6) provides a rough illustration of this process (note: LBNF will incorporate three horns in its design contrary to the illustration's two horns).

As the neutrinos and dark matter reach the Near Detector, they are met with huge array of detector instruments and target material. The bulk of the Near Detector is called the Fine-Grained Tracker (FGT) and consists of a straw-tube tracking detector, electromagnetic calorimeters (ECAL), and Muon Identifiers. It is designed to measure neutrino event rates and cross sections

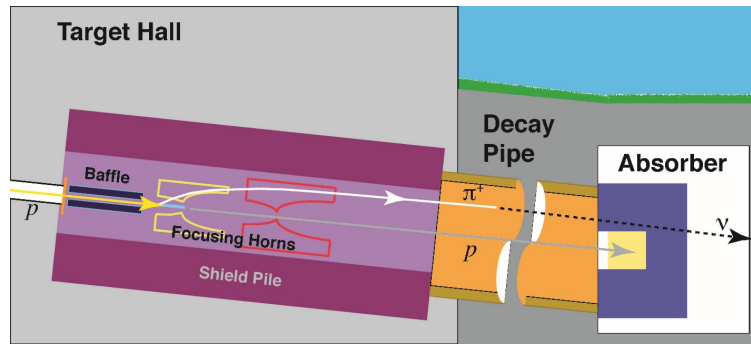


FIGURE 1.6: An illustration of the neutrino production mechanism (Note: three horns are used in LBNF rather than two).
From Ref. [4]

on argon, water, and other nuclear targets for both ν_e and ν_μ charged current (CC) and neutral current (NC) scattering events [5]. The heart of the detector is the straw-tube tracking detector which is designed to determine event vertex locations at high precision. It is made of straw tubes of outer diameter 1 cm where some of which are placed behind various argon and water targets and others behind Transition Radiator foils. The straw tube detector system is expected to contain 107,520 straws - making up 336 straws per plane, 1344 straws per module, and 80 modules which have electrical readout from both ends leading to 215,040 electronic channels and it is expected to weigh in at about 8 tons [5]. Surrounding the straw-tube tracking detector is a huge dipole electromagnet generating a field of 0.4 Teslas which will be used to induce Lorentz force on scattered charged particles and allow their momentum and charge to be measured. A schematic of the FGT is illustrated in Fig. (1.7).

Together with the ECALs, electron scattering energy and angle will be able to be measured at high precision and will be the focus of our analysis. Calculation of detection sensitivity via electron scatter events of dark matter in the Near Detector with the accompanying electron neutrinos as background will be discussed in the following chapters.

Lastly, neutrinos will travel 800 miles through the crust of the earth to

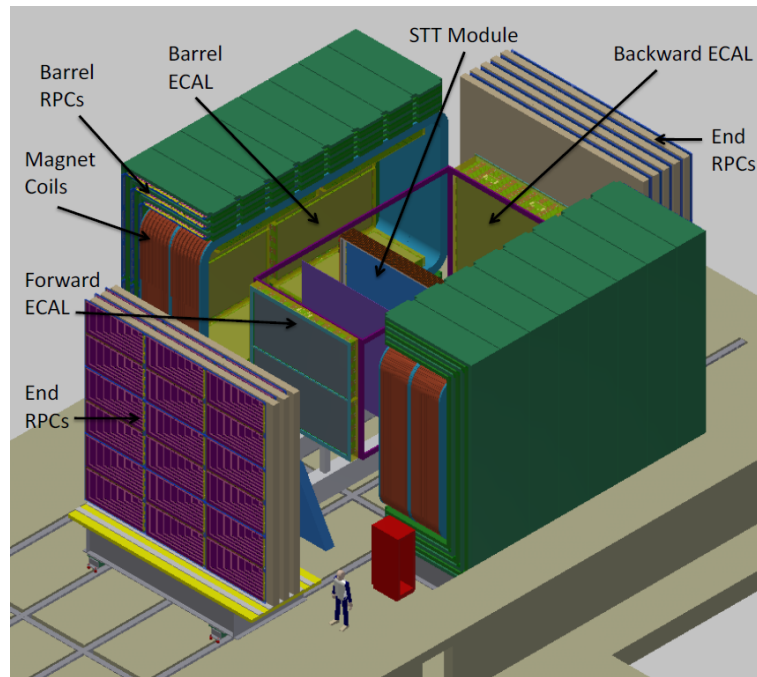


FIGURE 1.7: An illustration of the Fine Grained Tracking system proposed for DUNE. From Ref. [5]

four 10-kt LArTPCs at the far detector at the Sanford Underground Research Facility where they will be observed and hopefully their flavor will have oscillated as predicted. Signals acquired from each detector will be analyzed and tests to previously stated theories will finally be performed.

Chapter 2

Dark Matter Theory

Dark matter has only been observed indirectly and its identity as a particle, if it has one, is still unknown. It is not even known if it interacts with ordinary matter in any other force besides gravity. There are a few theories and models that attempt to describe dark matter. This chapter will focus on the Light Dark Matter model which is the model considered in our analysis. There have also been some experiments in recent years that have attempted to detect dark matter and, while unsuccessful, have imposed various new limits on the possible dark matter parameters which will also be discussed. As I am not proficient with theoretical particle physics, I'll try to avoid going too deeply into details of the theory. The reader is encouraged to check with the references if they wish to explore further.

2.1 Theoretical Background

Many gravitational phenomena in the large scale of the universe suggest the existence of a new unseen particle, dark matter. The question remains however, whether or not dark matter particles interact with ordinary matter in non-gravitational forces. From observations of dark matter thermal freeze-out, their relic abundance indicates they have weak-scale masses and order-one couplings [13]. Direct detection experiments of dark matter in the halo of the Milky Way recoiling off of underground detector nuclei in the past years

utilizing variations in velocity of Earth as it orbits the sun in reference to the orbit of the solar system in the galaxy have so far not resulted in a detection but have imposed strong constraints on dark matter with mass larger than 5GeV [14]. Lower mass dark matter however loses sensitivity in these experiments quickly due to the limited velocity variations of earth's orbit and yield very low recoil energies against nuclei. Low mass dark matter also begins to go below the Lee-Weinberg bound at which point the thermal relic needs non-Standard Model annihilation channels through light states to maintain their correct abundance [6]. Therefore we explore the use of a light mediator coupled to the standard model that allows production of sub-GeV dark matter.

2.2 Light Dark Matter Model

To model it, we extend the Standard Model gauge group by including a new $U(1)'$ group where the quarks are charged and leptons neutral. The $U(1)'$ gauge symmetry is spontaneously broken in a hidden sector and provides a minimal light dark matter model with Standard Model interactions included through kinetic mixing with the hypercharge gauge boson [7, 15–18]. This leads to a massive dark photon, V_μ of mass m_V and charge or baryon number q_B . We then introduce the dark matter and anti dark matter candidate, χ and $\bar{\chi}$, of mass $m_\chi < m_V/2$ since they are the daughter particles of V and we only consider on-shell production. It is a color singlet and electrically neutral except under $U(1)'$ where it has charge q_χ which we set to 1 and can be taken as a scalar or fermionic field. The Lagrangians are given by Eq. (2.1),

$$\mathcal{L} = \mathcal{L}_\chi - \frac{1}{4}V_{\mu\nu}V^{\mu\nu} + \frac{1}{2}m_V^2V_\mu V^\mu - \frac{\kappa}{2}V^{\mu\nu}F_{\mu\nu} + q_B\alpha V_\mu J_B^\mu + \dots \quad (2.1)$$

$$\mathcal{L}_\chi = \begin{cases} i\bar{\chi}\not{D}\chi - m_\chi\bar{\chi}\chi & \text{if Dirac fermion dark matter} \\ |D_\mu\chi|^2 - m_\chi^2|\chi|^2 & \text{if complex scalar dark matter} \end{cases} \quad (2.2)$$

where the χ and V_μ donate the dark matter and $U(1)'$ vector boson mediator with field strength $V_{\mu\nu}$ and covariant derivative $D_\mu = \partial_\mu - iq_\chi\alpha V_\mu$. α is the $U(1)'$ gauge coupling, $F_{\mu\nu}$ is the hypercharge field strength, κ is the kinetic mixing constant between the mediator and hypercharge field, and J_B^μ is the baryonic current. The \not{D} is Feynman slash notation and is defined as,

$$\not{D} \stackrel{\text{def}}{=} \gamma^\mu D_\mu$$

where γ^μ are the gamma matrices. In our analysis we are considering a fermionic dark matter particle with a purely 'Vector portal' mediator. Therefore, we take \mathcal{L}_χ equal to the Dirac fermion case in Eq. (2.2). This also sets q_B to 0 and introduces another coupling into the Lagrangian of $V^\mu(\alpha J_\mu^\chi - \kappa\alpha_e J_\mu^{EM})$ where J_μ^χ is the $U(1)'$ current for fermionic dark matter with $J_\mu^\chi = i\bar{\chi}\gamma_\mu\chi$ and $\alpha_e J_\mu^{EM}$ is the electromagnetic current with $J_\mu^{EM} = \sum_f e_f \bar{\psi}_f \gamma_\mu \psi_f$ summing over fermions of electric charge e_f and α_e is the fine structure constant $\sim 1/137$ [6, 7].

This Lagrangian introduces four new free parameters that may be varied for our sensitivity analysis: m_V - the mediator mass, m_χ - the dark matter mass, κ - the kinetic mixing, and α - the $U(1)'$ gauge coupling. We wish to present our sensitivity in 2 dimensions so we impose the constraints $m_V = 3m_\chi$ and $\alpha = 0.5$. Finally, we consider the range of m_χ to be between 50 MeV and 7 GeV and the range of κ to be between 10^{-4} and 10^{-2} . These constraints follow Ref. [19] and are conservative benchmarks that follow from the Relic Density and various other experiments.

2.3 Production

The V boson may be produced by proton scattering against a fixed target and propagate with a mass of 1 – 10 GeV as long as the proton energy is larger than a few tens of GeV. The main injector at Fermilab which is capable of energies 60 – 120 GeV is ideal for testing this range of V and may produce dark matter with high enough energy to generate neutral-current electron scattering events in the near neutrino detector [13]. Due to the high energy regime we are in, we only consider the parton level or ‘direct production’ process,

$$p + N \rightarrow V^* \rightarrow \chi^\dagger \chi$$

with leading order diagram shown in Fig. (2.1) [6].

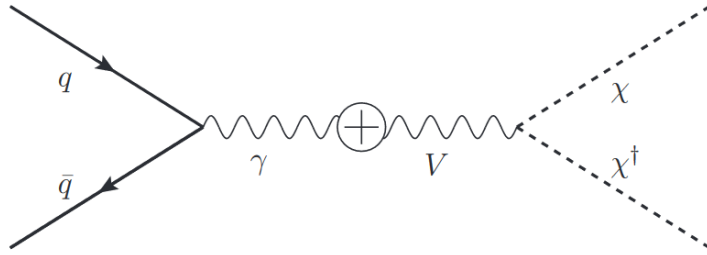


FIGURE 2.1: Dark matter direct production Feynman diagram.
From Ref. [6]

This process can be approximated using the ‘narrow width approximation’. The cross section for production of the dark matter is then written as,

$$\sigma(pN \rightarrow V^* \rightarrow \chi^\dagger \chi) = \sigma(pN \rightarrow V) \text{Br}(V \rightarrow \chi^\dagger \chi)$$

with $\text{Br}(V \rightarrow \chi^\dagger \chi) \sim 1$

$$\sigma(pN \rightarrow V) = \int_{\tau}^1 dx \frac{d\sigma(pN \rightarrow V)}{dx} \quad (2.3)$$

$$= \frac{4\kappa^2 \alpha_e \pi^2}{m_V^2} \sum_q e_q^2 \int_{\tau}^1 \frac{dx}{x} \tau [f_{q/p}(x) f_{\bar{q}/p(n)}(\frac{\tau}{x}) + f_{\bar{q}/p}(x) f_{q/p(n)}(\frac{\tau}{x})] \quad (2.4)$$

where the summation over q is over all quarks where e_q is the quark charge in units of positron electric charge, $\tau = m_V^2/s$ where \sqrt{s} is the hadron-level center-of-mass energy, and $f_{q/p(n)}(x)$ represents the parton distribution function (PDF) - estimates of which are obtained from CTEQ6.6 [6, 20]. The resulting differential production cross section as a function of the lab frame energy, E_χ , and angle between its lab frame momentum and the beam direction, θ , can be written as,

$$\frac{d\sigma(pN \rightarrow V \rightarrow \bar{\chi}\chi)}{dE_\chi d\cos\theta} = \left[\frac{\partial(x, \cos\hat{\theta})}{\partial(E_\chi, \cos\theta)} \right] \frac{d\sigma(pN \rightarrow V)}{dx} \text{Br}(V \rightarrow \bar{\chi}\chi) g(\cos\hat{\theta}) \quad (2.5)$$

where $\hat{\theta}$ is the angle between the momentum of χ and the beam direction in the V rest frame, $\left[\frac{\partial(x, \cos\hat{\theta})}{\partial(E_\chi, \cos\theta)} \right]$ describes the Jacobian attached to the change of variable of θ to $\hat{\theta}$, and the function g is the angular distribution of dark matter in the V rest frame which for dirac fermionic dark matter is $g(\cos\hat{\theta}) = \frac{3}{8}(1 + \cos^2\hat{\theta})$ [6].

2.4 Detection

Detection of the produced dark matter particles is possible by elastic electron scattering in the Near detector via neutral current interactions. Fig. (2.2) illustrates this process.

The electron scattering differential cross section takes the form,

$$\frac{d\sigma_{\chi e}}{dE_e} = 4\pi\kappa^2\alpha\alpha_e \frac{2m_e E_\chi^2 - (2m_e E_\chi + m_\chi^2)(E - m_e)}{(E^2 - m_\chi^2)(m_V^2 + 2m_e E_e - 2m_e^2)^2} \quad (2.6)$$

where E_e is the recoiling electron energy, E_χ is the incoming dark matter energy [6].

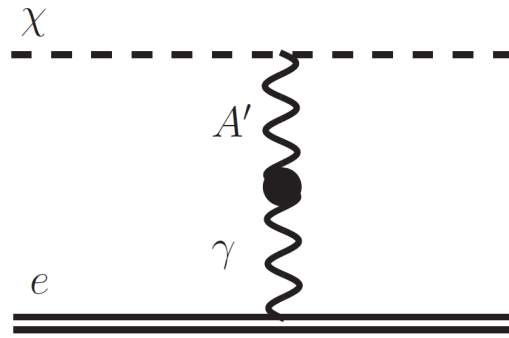


FIGURE 2.2: Dark matter neutral current elastic scattering from electrons. From Ref. [7]

In this analysis, we only analyze the signal and background of electron scatter events. The signal is of course the elastically scattered electrons via dark matter and background is elastically scattered electrons via electron neutrinos. Scattered electrons' scattering angle and energy can be reconstructed in the Near detector so we consider these two kinematic parameters for distinguishing our signal and background.

The simulation of these processes are described in Ch. (3) and the resulting signals are presented in Ch. (4).

Chapter 3

Experimental Setup

This chapter will discuss the simulation procedures that have been used for analysis of simulated light dark matter in the Deep Underground Neutrino Experiment (DUNE).

3.1 Software Simulation

The simulation of dark matter at DUNE is done in several steps, each of which will be discussed in detail. For this process, the Fermilab computing facility was used and several scripts and programs had to be used or made specifically for this experiment. The steps for the simulation process and analysis are shown in Fig. (3.1) and are described in the following sections,

The dark matter branch of this pipeline is repeated for every dark matter parameter set that we test. Since we are searching the threshold of 90% sensitivity over the range of the dark matter parameter space, we compute the dark matter production, propagation, detection, and sensitivity for each set of parameters and plot the 90% sensitivity threshold as a function of the free parameters. More on this in Ch. (5).

3.1.1 Fermilab Computing Grid

Because Monte Carlo is heavily employed in the simulations, powerful computing power is a must since Monte Carlo relies on repeated random sampling for numerical results. For this reason, we chose to design our simulation software pipeline to use the Fermilab computing grid. The computing grid allows physicists to submit and run a large batch of processes on a network of shared computing resources. Fermilab's grid resources are all organized into a single architecture called FermiGrid Gateway [21]. Jobs submitted will either be chosen to run on the FermiGrid Gateway where Fermilab's own nodes will process the job, or they may be outsourced to various institutions or other computing centers via the Open Science Grid e.g. Tera Grid or EGEE.

After acquiring credentials from Fermilab, the computing resources are able to be employed for our experiment. Their interactive nodes can be accessed through ssh and the Kerberos protocol to various general purpose virtual machines (gpvm). The address of the ones accessed by our group are `dunegpvmXX.fnal.gov`, where XX represent the virtual machine number, 01 – 10. Each machine runs Scientific Linux, a free Linux distribution based on Red Hat Enterprise and produced at Fermilab. The root filesystem contains many different mount points accessible to users and lead to different storage systems at Fermilab. Those used for our experiment are as follows,

/dune/app

Stored locally on Fermilab's BlueArc disks – Limited space and used for mainly for user's executables.

/dune/data

BlueArc storage partition for experiment data – More space than 'app' but still limited

/pnfs/dune

dCache storage – Nearly unlimited storage but slow. Computing batch nodes only have access to this storage system.

Therefore, all our software for heavy computation and scripts for submitting them are stored in `/dune/app`. When it's time to do work, resources and executables required for the computing processes are copied to `/pnfs/dune` and results from the computations are stored in `/pnfs/dune`. When we're ready to analyze the data, it is copied to `/dune/data`, tarred, and downloaded for local analysis. There are a few tools developed by Fermilab that are required for using the computing cluster; they are 'jobsub', 'ifdh', and 'setup'.

'Jobsub' is Fermilab's job management software that allows submitting new jobs or removing, pausing, unpausing, or querying already submitted jobs. It is written in python and communicates with Fermilab's jobsub server via http. Submitting a group of jobs only requires the number of jobs, the user's group, the expected lifetime of the process, and the path to the script file containing the commands to run the process. 'ifdh' is the most common tool used for transferring files between mount points on the Fermilab grid. It picks out the best protocol for file transfer and manages the transfer until completion. Finally, 'setup' prepares the node's environment with requested software dependencies from Fermilab's local software repositories. The user can request various versions, os's, or features of various software dependencies and it will set up their environment with that requested software. For example, our project requires setting up 'ifdh', 'python', 'gcc', 'jobsub', and 'root'.

To manage all of Fermilab's tools and job handling, I developed a python script to streamline the process. It takes a list of dark matter parameter sets and generates the required configuration for a dark matter production simulation given each parameter set, then transfers the generated files to the dCache where worker nodes can access them, generates the script file that

each worker node will use to complete each job, and then submits the jobs with `jobsub` to be ran. Once the jobs are all completed we transfer the data to `/dune/data` and put it in a tarball to be downloaded for local analysis. The script also contains useful functions for generating parameter sets, for example it can generate an N-dimensional linearly or logarithmically spaced grid of parameters given a range and number of points where N is the number of free parameters. It can also take a set of parameters via file for generation. One technique implemented is to generate points around a sensitivity contour from a previous run and use them to refine the contour. The script can be found in Appendix (A).

3.1.2 MadGraph5

To generate event data of dark matter produced in the DUNE target, we utilize the `MadGraph5_aMC@NLO` particle event generation software [22]. <http://madgraph.physics.illinois.edu/>. It is free software developed internationally to perform computations of tree-level and leading order (LO) or next-to-leading order (NLO) cross sections of nearly any standard model or beyond the standard model process. It merges into a unique framework all of `MadGraph5`'s and `aMC@NLO`'s features using a python interface, and includes some of its own features such as the merging of event samples with different light-parton multiplicities. It has been designed for ease of use by physicists not familiar with Quantum Field Theories specifically QCD.

To perform calculations with this software, all the user must do is provide `MadGraph5_aMC@NLO` with the theory model and its parameters, such as Lagrangian of the theoretical model plus its couplings and masses. This is done via Fortran code and is packaged into a folder containing all of the other settings and parameters used for simulation. The model package we used is a

Light Dark Matter model package provided by Dr. Chris Jackson and it incorporates all of the theory for the production of Light Dark Matter as discussed in Ch. (2). Next we start the `mg5_aMC` executable which is an interactive terminal that allows us to specify which processes to analyze. We first import the Light Dark Matter model, and since we're only concerned with the direct production of dark matter via proton collision, we specify analysis of the $p + p \rightarrow \chi + \bar{\chi}$ process. The executable then copies the Fortran code from the model along with all other required internal computation code and packages them all into a folder where the simulation can be performed. Within this package, the executable 'madevent' is used to configure the simulation, compute the events, and combine them into a single event data file. With this executable, we configure the masses, coupling, and mixing constants to the parameter set we wish to simulate, the beam energy and composition, and the number of events to simulate. Since we wish to simulate a proton beam on a proton fixed target, we choose the beam to be composed of protons with one beam at the desired beam energy and the other at the proton rest mass energy. We also configure 'madevent' to package the simulation into what is known as a 'gridpack' which is just a tarball that can be sent to a computing node, unpacked, and executed.

After our script runs `madevent` and produces the gridpack, the gridpack is copied to `dCache` and a batch of jobs are submitted to execute the gridpack in parallel among many different computing nodes. Each node is assigned a process number which is used to set the random seed for each simulation. We run 200,000 events on each job with 250 total jobs submitted for a total of 50,000,000 dark matter events. Fig. (3.2) shows the computing statistics provided by FIFEmon for a batch of 250 jobs. The minimum, maximum, and average of each statistic of all the jobs is shown where Memory and Disk are the RAM and disk space used by the simulation, Wall Time and CPU Time are the total time used and the CPU time used (copying to and from the

dCache is quite slow which is why we see such a large difference between the two), CPU and Time are the CPU usage percent and the time taken vs the predicted time taken, and lastly Exit Code is whether or not the script terminated successfully and 0 is successful. After the gridpack has successfully generated the particle events, we use a modified executable from the ExRootAnalysis library to discard events that do not propagate to the near detector and output the resulting particle event data into a ROOT NTuple. We also save MadGraph's calculated production cross section of the process in the ROOT file so it can be used later for weighting. ROOT is a data analysis framework developed by CERN and its NTuple format is very disk space and CPU efficient. Calculating propagation of the particles to the near detector and discarding the ones that don't make it there will be discussed in more detail in the DuneDM subsection; doing this reduces the file size of the dark matter events significantly. Even though some events are discarded, we still keep histograms of all event's various kinematic parameters within the ROOT file for later analysis, more on that in the DuneDM subsection as well. Finally, the resulting root file is copied to the dCache where it can be sent to /dune/data and tarred for download.

3.1.3 G4LBNE

Neutrino simulation at DUNE is achieved using Fermilab's own simulation package, G4LBNE <https://cdcvns.fnal.gov/redmine/projects/lbne-beamsim/wiki>, and is used specifically for optimization of neutrino flux. This software simulation is built upon the GEANT4 framework, which is a Monte Carlo high energy particle physics simulation framework. In this simulation, the proton beam is defined to match the input beam from the Main Injector, the fixed target is defined as a graphite block that the beam impacts, the magnetic horn fields are also defined and deflect the charged pions and kaons,

and then it uses ‘dk2nu’, a software package designed to simulate neutrino production more accurately using the decays of the kaons and pions and newer ‘Beyond the Standard Model’ physics calculations. A wireframe rendering of the simulation is shown in Fig. (3.3). The team at Fermilab runs this simulation repeatedly with tweaks to various parameters of the beamline, such as horn positions, horn geometry, horn current, beam energy, etc. to maximize the output neutrino flux. Over the years, they have published several configurations resulting in optimal neutrino flux in the DUNE concept design reports. We use the latest configuration so that we match the DUNE experiment as closely as possible. Because the fluxes are generated with Monte Carlo, again, there is a costly computation time. Thankfully, the team at Fermilab has already integrated it to be used with the Fermilab computing cluster. The only effort we have to do is input the number of jobs, number of protons on target, and the beamline configuration file and then run their job submission script. The output can then be retrieved from dCache and downloaded locally to be used with our analysis.

3.1.4 DuneDM Detector Signal

Once neutrino and dark matter event data is downloaded, we can proceed with the next step of the analysis which is to read the event particles’ kinematics, propagate them to the Near Detector, and generate a signal. To do this, we developed a standalone application called DuneDM <https://github.com/thegrb93/DuneDM> with C++ and a few other libraries including ROOT and dk2nu. The dark matter and neutrino particle kinematics are stored in a cluster of .root files since each computing node copies its output individually to the dCache and we don’t worry about combining them into a single .root file. To read these files, we simply execute DuneDM with the command line arguments set to the path of the folder containing the cluster of .root files and

it will read each `.root` file inside that folder. For dark matter folders, the name of the folder must also contain the parameters of the dark matter in this pattern: `'DM_m_V_m_χ_κ_α'`. The job generation script should handle this automatically. This allows DuneDM to also read the parameters of the generated dark matter since altering the simulation pipeline to store them in the `.root` files would prove too cumbersome.

The path to the neutrino folder is specified with the `--neutrinos` option, the path to the dark matter folders are specified as positional arguments, and setting the 'mode' of DuneDM is done with the `--mode` option. There are two modes implemented in DuneDM: 'detector' which will simulate the propagation and detector signals of neutrinos and dark matter and generate distribution plots of the kinematics of each stage (more on this in Ch. (4)), and 'sensitivity' which will propagate and generate detector signal for neutrinos and each dark matter positional argument and then calculate the sensitivity of each and then plot the 90% sensitivity threshold contour (more on this in Ch. (5)).

As each dark matter `.root` file is read, the number of events in each file is attained and DuneDM iterates over each event reading the kinematic parameters of each particle. We acquire the dark matter parameters from the folder name as mentioned earlier and the four-momentum of the produced dark matter and anti-dark matter is read. After acquiring the four-momentum of the particles, the next step is to ensure that the particle propagates to the fiducial volume of the Near Detector. In this step, we neglect interactions with gravity and interactions with the earth's crust because the particles reach the detector in a matter of nanoseconds so the deflection due to gravity is negligible, and the interaction cross section of the particles is so small we assume no interaction with the crust. This simplifies our propagation model to a ray which we intersect with the fiducial volume of the Near Detector which is a 4m x 3m x 5m rectangular prism 575m downstream from the target. The

algorithm used for this test is a simple ray-box intersection algorithm known as Smit's ray-box algorithm [23]. This process is also carried out on the computing node during the processing of the event data from MadGraph to filter out events that miss the fiducial volume and reduce disk usage, but we do it again here to calculate the path-length of the particle through the box which is used in the scattering probability calculations. Reading each neutrino .root file is done similarly, but the structure of the data is somewhat different. In addition to saving the production neutrinos' kinematics, G4LBNE also stores the neutrino kinematics at each detector so the ray-box test is only done in order to calculate the path length of the neutrino through the detector.

Once we have the path length of the particle through the fiducial volume of the Near Detector, the next step is calculating the scatter probability of the particle within the detector volume and then, if it scatters, the resulting scattering angle and energy of both the dark matter or neutrino and the electron. We can calculate the scattering cross section of dark matter using Eq. (2.6). Using the dark matter parameters and energy, the cross section takes the form,

$$\sigma_{\chi,e}(E) = \int_{E_e^{min}}^{E_e^{max}} dE_e \frac{d\sigma_{\chi,e}}{dE_e} \quad (3.1)$$

where E is the dark matter energy and $E_e^{max/min}$ are the minimum and maximum electron recoil energy which for minimum is calculated as the recoil energy when the electron scatters with an angle $\pi/2$ with respect to the dark matter momentum and maximum when it scatters with an angle of 0 with respect to dark matter momentum [7]. Those scatter energies are calculated as a function of the dark matter mass and energy using momentum and energy conservation in an elastic scatter scenario. Using the integrated $\frac{d\sigma_{\chi,e}}{dE_e}$ from Eq. (2.6), we evaluate the integral at those two limits and finally have the

cross section. The scattering probability is then $\sigma_{\chi,e} ZL$ where Z is the electron number density of the detector which we estimate to be 5.1×10^{23} and L is the path length of the dark matter through the detector. With this probability, we take a uniform $(0 - P_{max})$ random probe, where P_{max} is the maximum probability calculated by the simulation that we keep updated as the simulation continues, and if the probability is greater than our probe, then we save it as a scattered event and weight the scatter by $\epsilon_{eff} P_{max}$ where ϵ_{eff} is the effective sensitivity of the detector which we estimate to be 0.9. For calculating the scattering kinematics, we take a uniformly random energy $(E_e^{min} - E_e^{max})$, calculate $\frac{d\sigma_{\chi,e}}{dE_e}$, and compare it to another uniformly random probe $(0 - \frac{d\sigma_{\chi,e}}{dE_e}(E_e^{max}))$. If the differential cross section is greater than the probe, then that is the scattering energy we use, and we calculate the scattering angle and momentum with it and a uniform random scattering azimuthal angle $(0 - 2\pi)$, otherwise, another random energy is taken and probed until the calculated differential cross section is greater.

Neutrino scattering is done exactly the same way except instead of using analytical formulas, we use estimated cross section data from GENIE as a function of the neutrino energy. This is done using linear interpolation and any neutrinos with energy too small to be interpolated are not scattered. The data was acquired from Ref. [24].

The final step of our calculations is to reweight the neutrino and dark matter distributions so that they correspond to the correct number of protons on target for the DUNE experiment. Since the DUNE experiment is expected to collide approximately 1.1×10^{21} protons on target per year for a 120 GeV beam (assuming a 100% duty factor), simulating this many events for every parameter set is computationally infeasible. For this reason, we scale the dark matter and neutrino distributions based on their calculated simulated protons on target vs. the DUNE experiment's protons on target. For the neutrino distributions, this is easy because we explicitly defined the number

of protons on target for the G4LBNE simulation. For dark matter however, we defined the number of events and MadGraph calculated the production cross section of the process afterwards. To calculate our simulated protons on target for the dark matter, we read the calculated production cross section from each .root file that was saved by ExRootAnalysis mentioned earlier and average them. Therefore the equation for calculating the protons on target is as follows,

$$N_p = \frac{N_\chi}{\sigma(pp \rightarrow \chi\bar{\chi})10^{-36}ZL} \quad (3.2)$$

Where N_p is the number of protons on target, N_χ is the number of dark matter events, $\sigma(pp \rightarrow \chi\bar{\chi}) \times 10^{-36}$ is the production cross section of our process converted from picobarns to cm^2 , Z is the proton density of the target (estimated to $12N_A$ for graphite) in cm^{-3} where N_A is Avogadro's number, and L is the length of the target in cm. After N_p is calculated, we scale the distribution by N_{DUNE}/N_p where N_{DUNE} is the expected protons on target of the DUNE experiment. Once dark matter and neutrinos have their respective scalings, histogram distributions of their kinematics at the different stages of the simulation: production, fiducial volume intersection, scattering in the detector, and scattered electrons in the detector are created and saved in .root format. Image plots of the histograms are also saved, including comparison plots between the neutrinos and dark matter in both linear and logarithmic scales. This is discussed in Ch. (4). Foreground and background electron scatter signal is also used to calculate sensitivity. This is discussed in Ch. (5).

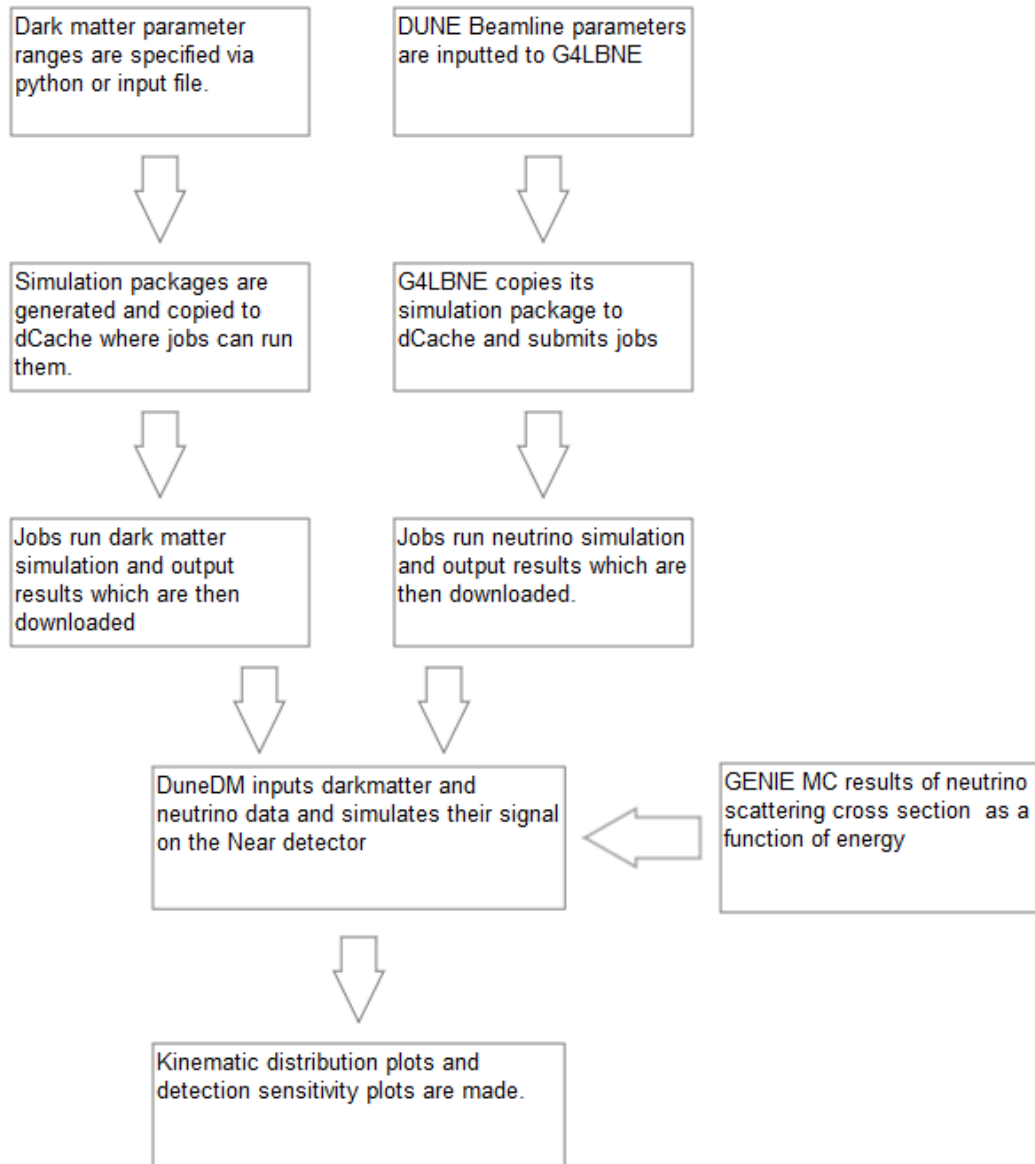


FIGURE 3.1: Block diagram of the simulation showing the steps needed to reach the final result.

Success rate (% jobs with exit code 0): 100.0%

Used	Min	Max	Avg
Memory	85.2 MiB	139.5 MiB	91.6 MiB
Disk	0.5 GiB	0.5 GiB	0.5 GiB
Wall Time	19m20s	2h23m25s	1h25m11s
CPU Time	15m34s	53m44s	31m13s
Efficiency	Min	Max	Avg
Memory	N/A	N/A	N/A
Disk	N/A	N/A	N/A
CPU	14.2%	99.2%	41.5%
Time	5.4%	39.8%	23.7%
Exit Code	# Jobs		
0	250		

FIGURE 3.2: Computing statistics of a batch of jobs on cluster machines reported by Fermilab's FIFEMon.

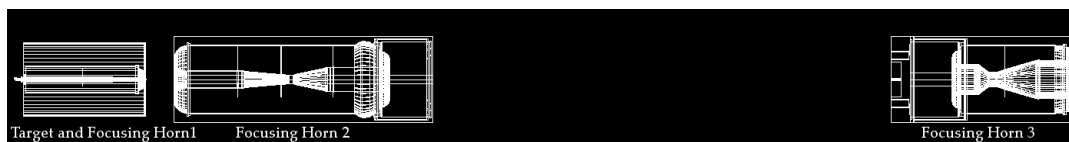


FIGURE 3.3: A rendering of the latest G4LBNE simulation models to date. The decay pipe and other containment volumes are not shown here.

Chapter 4

Simulation Results

In this chapter, the results of the simulation will be displayed as histogram plots of the kinematic parameters of dark matter and neutrinos at the different stages of the simulation: production, intersection with the fiducial volume, and scattering. As mentioned in Ch. (2), the two free parameters of dark matter are the m_χ and κ while $m_V = 3M_\chi$ and $\alpha = 0.5$. The proton beam energy in all of the results will be 120GeV and the number of protons on target corresponds to 3.5 years of operation at 1.2 MW power with 50% duty cycle or 1.925×10^{21} protons on target (POT). The distributions of kinematics of low and high m_χ with low and high κ will be presented in log scale histograms beside their respective normalized histograms. The kinematic parameters that will be shown are:

- The χ and ν_e energy at each stage as $E(\text{GeV})$.
- The χ and ν_e angle with respect to the beam direction at each stage as $\theta(\text{rad})$.
- The χ and ν_e angle with respect to the beam direction at each stage as $\theta(\text{rad})$ zoomed in.
- The χ and ν_e scattered electron energy $E(\text{GeV})$.
- The χ and ν_e scattered electron angle as $\theta(\text{rad})$.

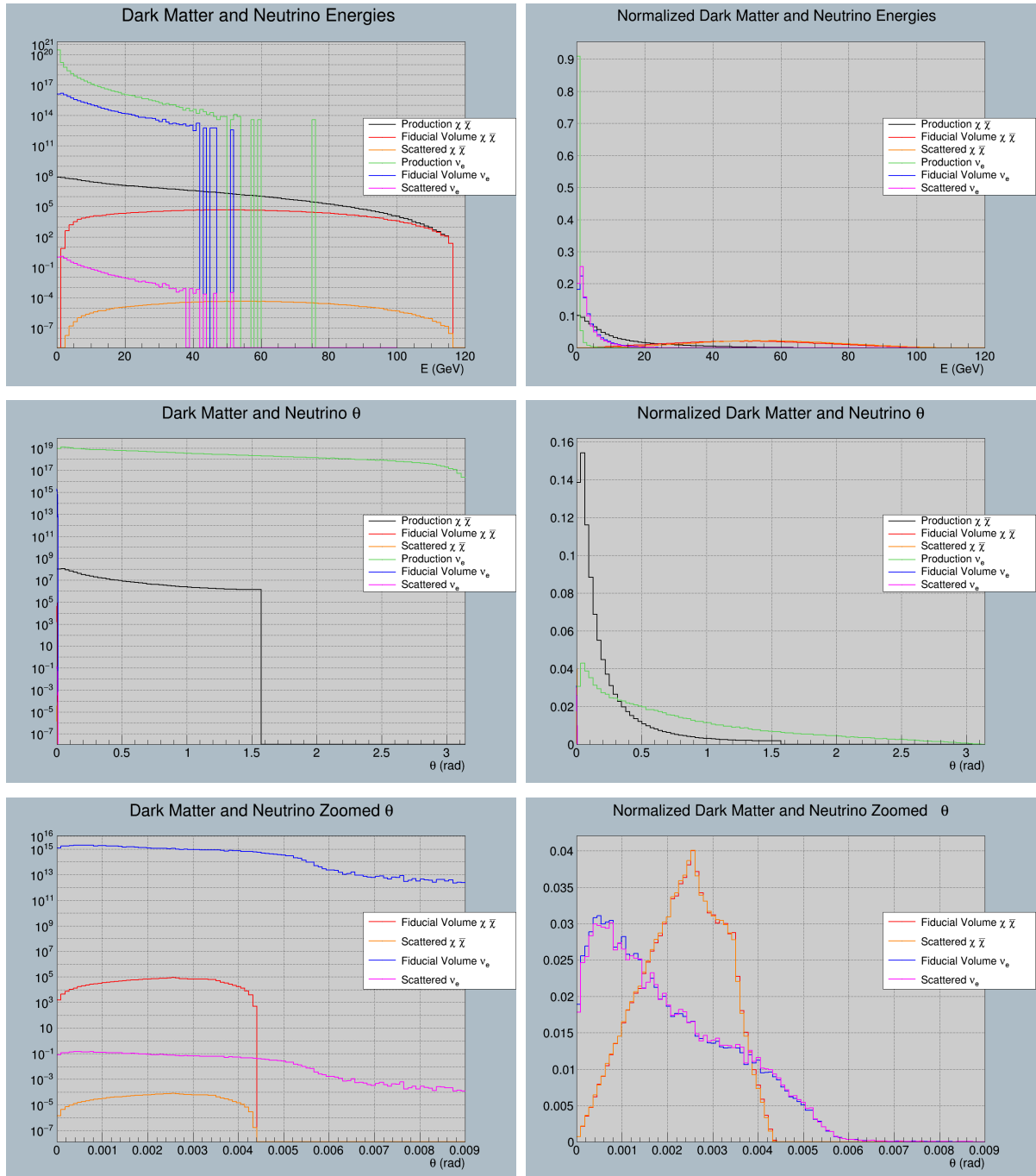


FIGURE 4.1: Dark matter and Electron Neutrino distributions at the stages of the simulation. Low mass dark matter $m_\chi = 50 \text{ (MeV)}$ with Low Kinetic Mixing $\kappa = 10^{-4}$

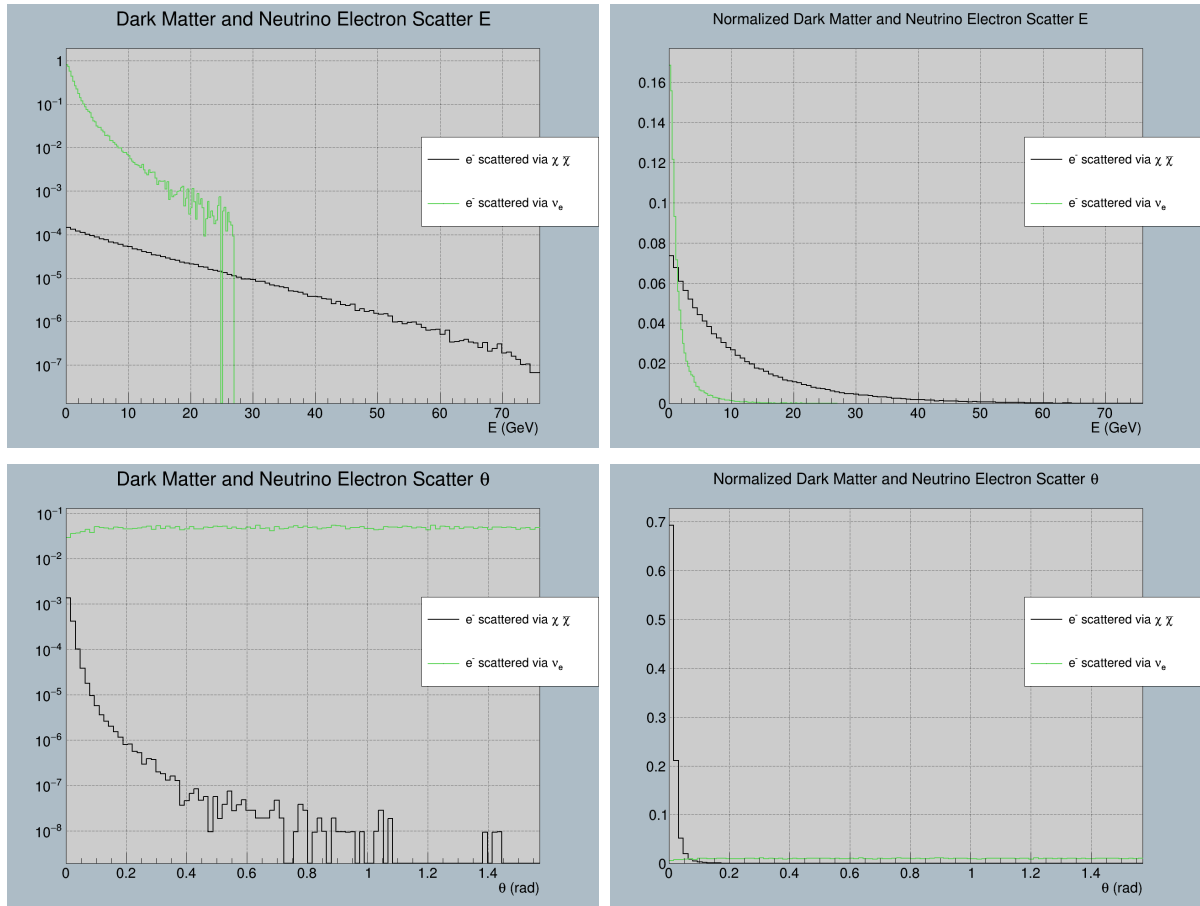


FIGURE 4.2: Electron signal from Dark matter and Electron Neutrinos. Low mass dark matter $m_\chi = 50(\text{MeV})$ with Low Kinetic Mixing $\kappa = 10^{-4}$

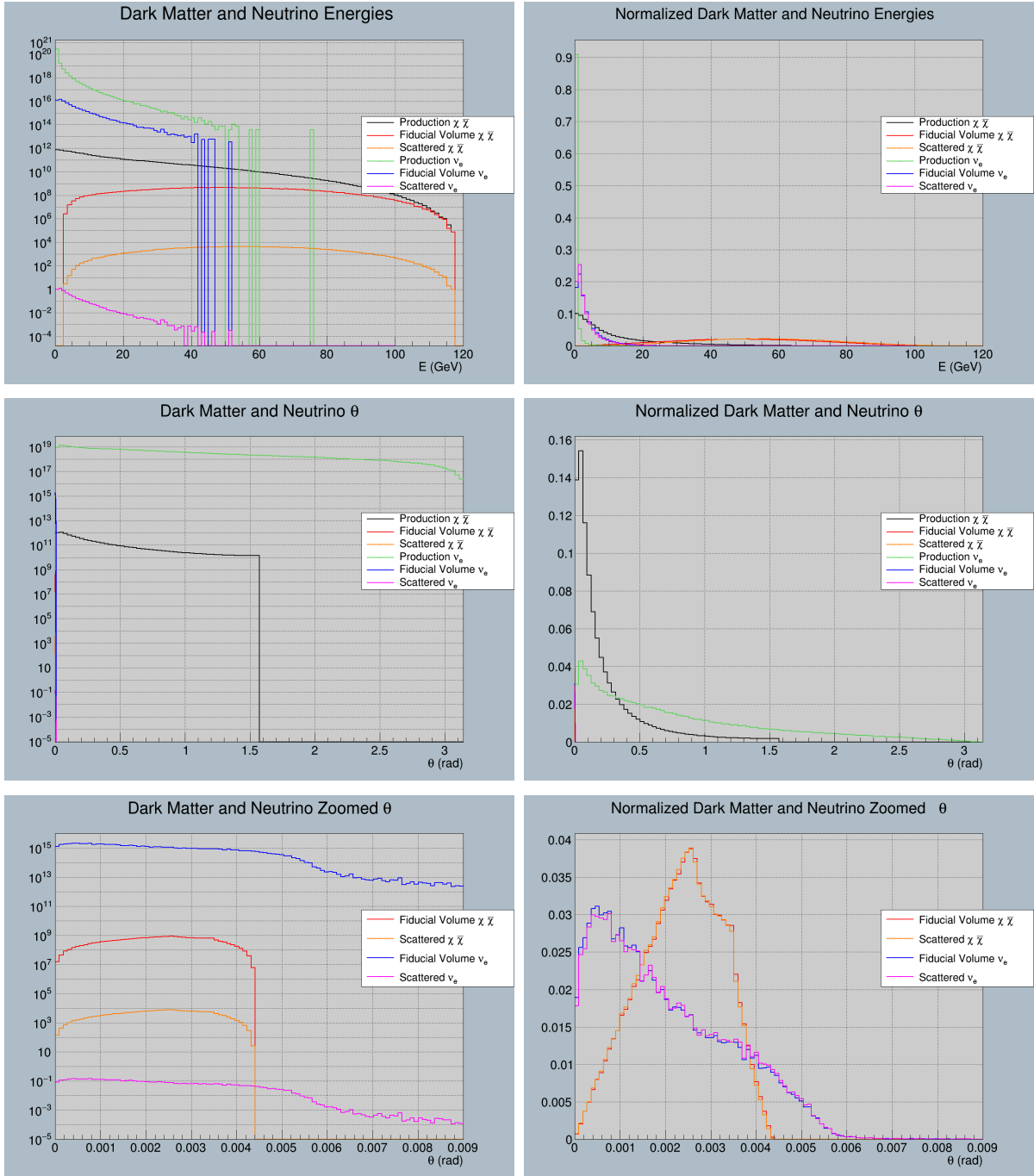


FIGURE 4.3: Dark matter and Electron Neutrino distributions at the stages of the simulation. Low mass dark matter $m_\chi = 50(\text{MeV})$ with High Kinetic Mixing $\kappa = 10^{-2}$

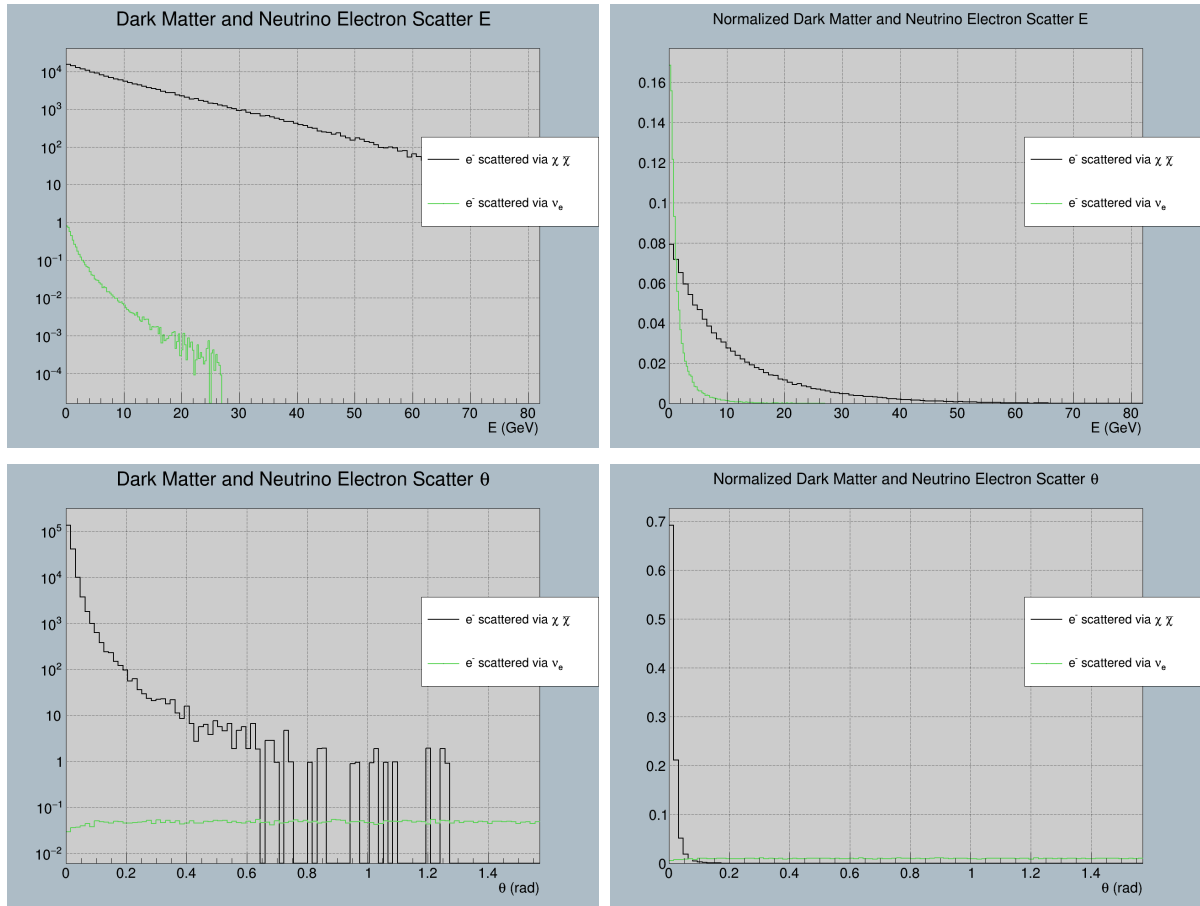


FIGURE 4.4: Electron signal from Dark matter and Electron Neutrinos. Low mass dark matter $m_\chi = 50(\text{MeV})$ with High Kinetic Mixing $\kappa = 10^{-2}$

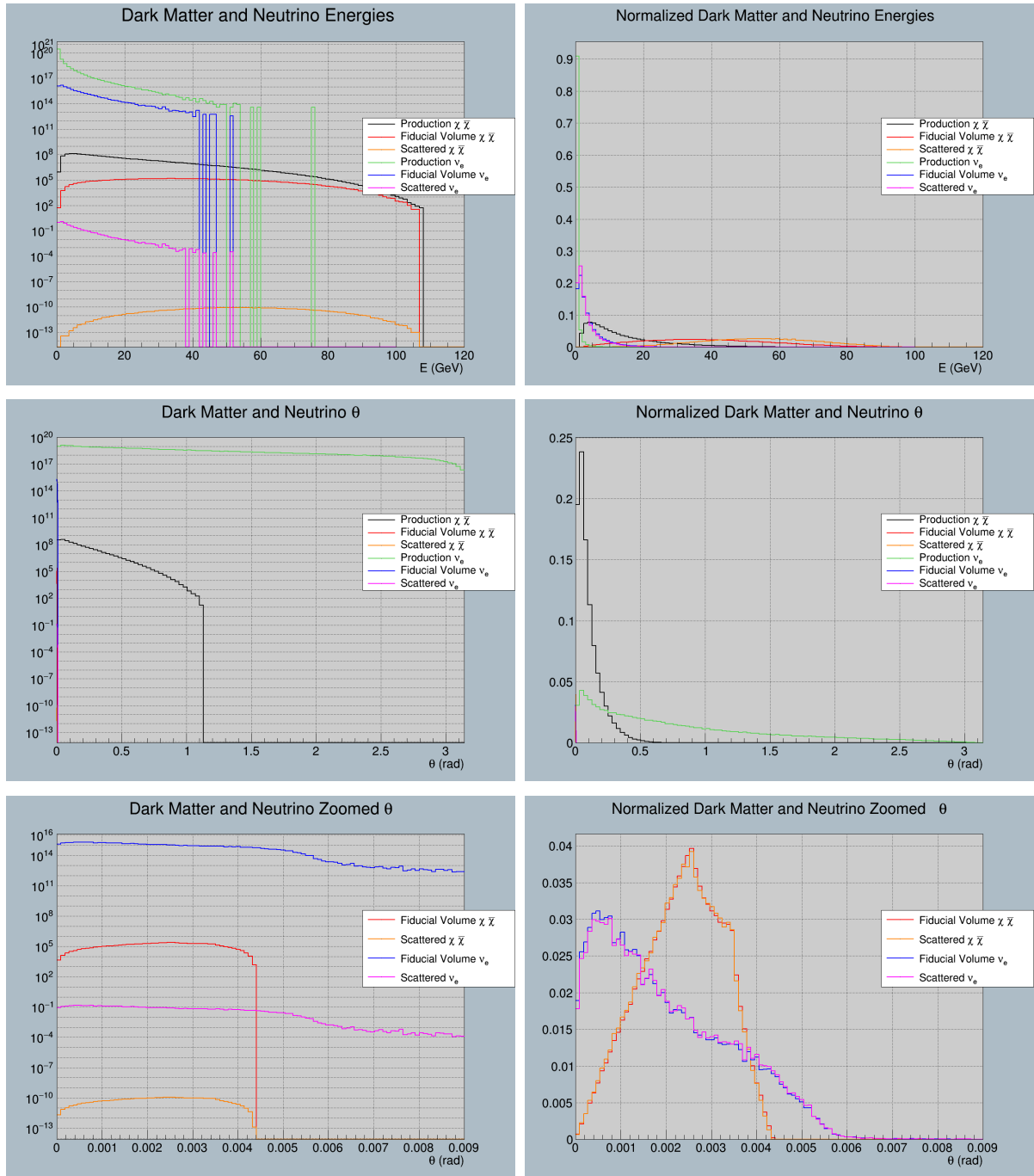


FIGURE 4.5: Dark matter and Electron Neutrino distributions at the stages of the simulation. High mass dark matter $m_\chi = 3(\text{GeV})$ with Low Kinetic Mixing $\kappa = 10^{-4}$

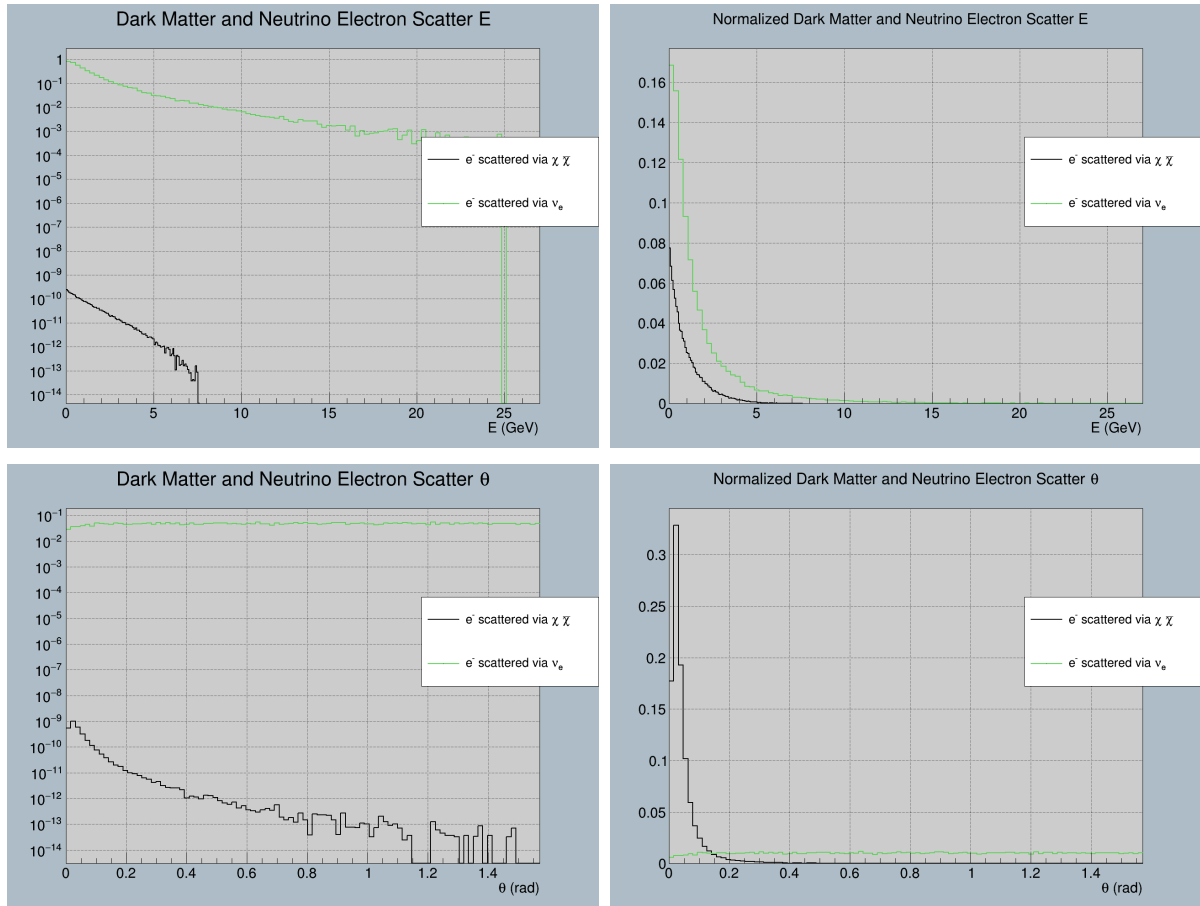


FIGURE 4.6: Electron signal from Dark matter and Electron Neutrinos. High mass dark matter $m_\chi = 3(\text{GeV})$ with Low Kinetic Mixing $\kappa = 10^{-4}$

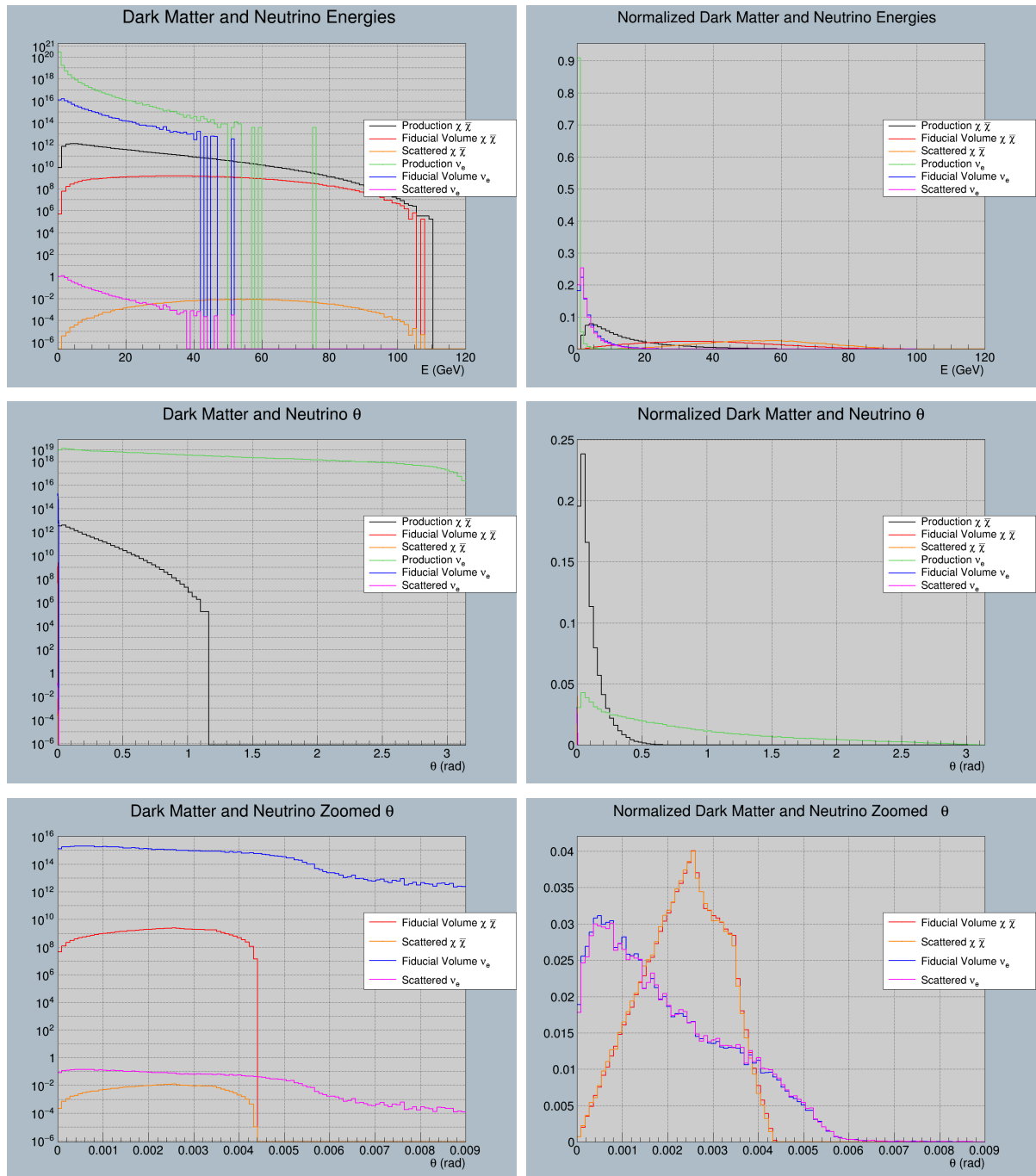


FIGURE 4.7: Dark matter and Electron Neutrino distributions at the stages of the simulation. High mass dark matter $m_\chi = 3(\text{GeV})$ with High Kinetic Mixing $\kappa = 10^{-2}$

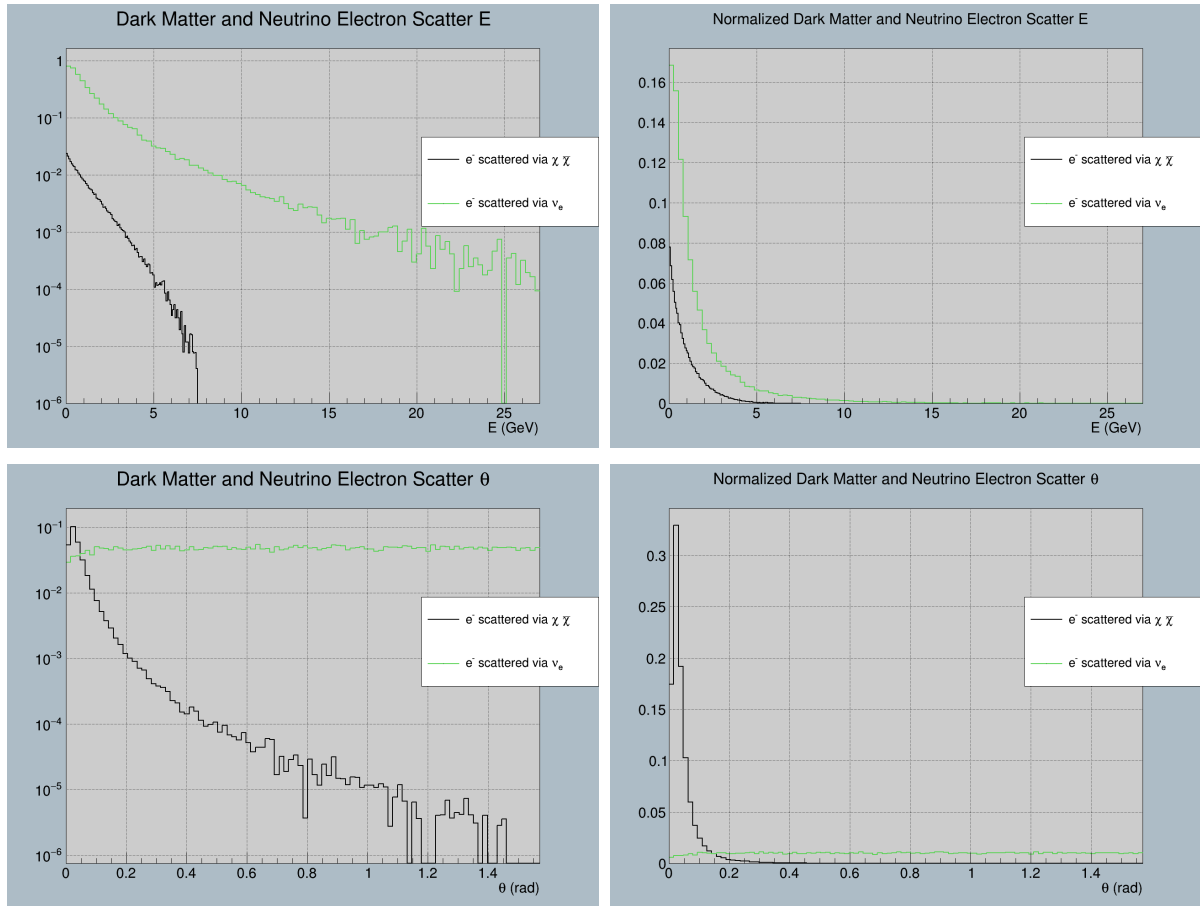


FIGURE 4.8: Electron signal from Dark matter and Electron Neutrinos. High mass dark matter $m_\chi = 3(\text{GeV})$ with High Kinetic Mixing $\kappa = 10^{-2}$

4.1 Observations

Immediately, we see a vast difference in the number of neutrinos and dark matter produced; in some areas over 8 orders of magnitude difference, however, electron neutrinos' energy appears to have a limit of around 60 GeV but dark matter energy ranges all the way to 115 GeV. Looking at the particles that intersected the fiducial volume of the detector, we can see that higher energy dark matter has a lower zenith angle with respect to the beam direction and has a higher probability of intersection - electron neutrinos exhibit this same characteristic. As for the probability of scattering, we see that electron neutrinos have a vastly lower chance of scattering than dark matter. This seems to balance the huge difference in number of particles. We also see that lower energy particles have a lower probability of scattering. Looking at the zenith angle of the particles, we see that dark matter production cuts off at $\pi/2$ whereas electron neutrinos are produced at any angle. In the zoomed in θ plot, we see the dark matter cuts off at about 0.0044 radians because this is the maximum angle that can reach the detector; the electron neutrinos seem to extend past this cut off a little bit because their trajectories are weighted and calculated in G4LBNE with Monte Carlo integration. G4LBNE also has slightly different detector dimensions than what the DUNE CDR proposes, but we dismiss these differences as negligible.

As for the scattered electron energy, it seems that lower mass dark matter can impart much more energy with much higher probability than higher mass dark matter and much greater energy than electron neutrinos. Their scattering angle also peaks near the forward scatter angle, but electron neutrino scatter angle is nearly evenly distributed.

The relation between dark matter distributions and the parameters of dark matter mass and kinetic mixing is also evident. A higher kinetic mixing constant leads to higher production of dark matter and higher probability of

scattering. Looking at the 50MeV mass dark matter with high kinetic mixing, we see a massive boost in detector signal to the point of it exceeding the background signal significantly. Higher mass dark matter results in a lower zenith angle and higher probability of reaching the detector, however it also decreases the probability of scattering significantly.

Chapter 5

Sensitivity

5.1 Calculation

In this chapter, the results of the χ^2 analysis are explained and presented. We study the χ^2 sensitivity to the parameter space: Y vs. m_χ where Y is,

$$Y \equiv \kappa^2 \alpha \left(\frac{m_\chi}{m_V} \right)^4$$

which illustrates the parameter scaling of the annihilation and scattering cross sections and assists the comparison with direct detection sensitivity [7]. Conventionally the parameter space is constrained with $\alpha = 0.5$ and $m_\chi/m_V = 1/3$ and we follow this convention to compare with other experiments.

For our χ^2 study we take into account the smearing of energy in the FGT near detector. To smear energy, we use the predicted smearing of 5% presented in the DUNE CDR with a Gaussian resolution function,

$$R(E_t, E_m) = \frac{1}{\sqrt{2\pi}\sigma} \exp\left[-\frac{(E_m - E_t)^2}{2\sigma^2}\right]$$

where E_m and E_t are the measured and true energies and σ is smearing width $\sigma = 5\%/\sqrt{E_t}$ [5, 25]. To construct E_m , we just use the equation $E_m = E_t + R_{norm}(E_t, \sigma)$ where R_{norm} is a random number generated via a normal

distribution centered at E_t with width σ . Then E_m is binned in a histogram with 20 bins from 0.3 to 15 GeV.

To calculate χ^2 , we denote N_i^{th} as the i 'th energy bin containing both dark matter and neutrino events, and N_i^{ex} as the i 'th energy bin containing only neutrino events. Since each bin contains more than 5 events, we use Gaussian error analysis. For the statistical uncertainties we can calculate

$$\chi_{stat}^2 = \sum_{i=E_m \text{ bins}} \frac{(N_i^{ex} - N_i^{th})^2}{N_i^{ex}}$$

However, we must account for theoretical and systematic uncertainties. We use the same uncertainties from Ref. [25] for a water based neutrino detector but they may need adjusting in the future to better match the DUNE near detector. They are: a flux normalization error of 20%, a tilt factor uncertainty of 5%, a zenith angle dependence uncertainty of 5%, an overall cross section uncertainty of 10%, and an overall systematic uncertainty of 5%. To account for these errors in χ^2 , we use adopt the 'method of pulls' [25]. In this method, N_i^{th} is extended to,

$$N_i^{th} = N_i^{th}(std) + \sum_{k=1}^{npull} c_i^k \tilde{\zeta}_k$$

where $N_i^{th}(std)$ is the theoretical rate for bin i , $npull$ is the number of sources of uncertainty which is 5, $\tilde{\zeta}_k$ are the 'pull' variables of which are free to be varied, and c_i^k is the change in N_i^{th} as the k 'th source of error changes per 1 standard deviation. Since the uncertainties are not large we consider the changes to be linear in $\tilde{\zeta}_k$ and our χ^2 is thus modified to

$$\chi^2(\tilde{\zeta}_k) = \sum_i \frac{(N_i^{th}(std) + \sum_{k=1}^{npull} c_i^k \tilde{\zeta}_k - N_i^{ex})^2}{N_i^{ex}} + \sum_{k=1}^{npull} \tilde{\zeta}_k^2$$

where the additional sum of $\tilde{\zeta}_k^2$ is a penalty imposed for moving each input

away from its standard value. The minimum χ^2 with all theoretical and systematic uncertainties is then obtained by minimizing $\chi^2(\xi_k)$ with respect to all pulls:

$$\chi_{pull}^2 = \operatorname{argmin}_{\xi_k} (\chi^2(\xi_k))$$

5.2 Results

χ^2 is computed for each set of two dark matter parameters (Y vs m_χ) and plotted as a 3D surface. We use ROOT to interpolate this surface and to generate a contour where this surface meets $\chi^2 = 90\%$. The result is plotted below in Fig. (5.1). We then imposed this plot on top of results from various other analyses, from Ref. [7], to compare with DUNE shown in Fig. (5.2) as a dark green contour. The black contour represents the relic density which provides the absolute limit to the parameter space of dark matter and is based on the produced dark matter in the universe.

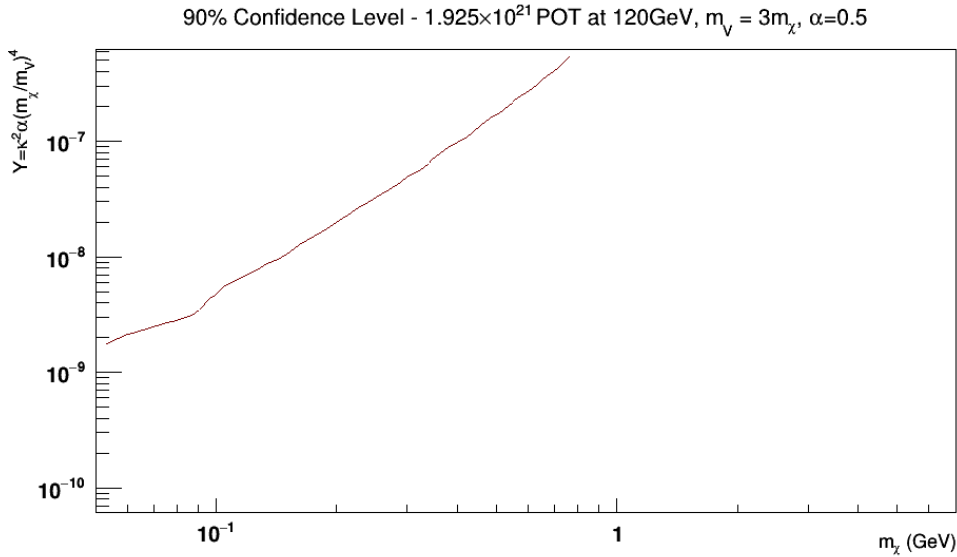


FIGURE 5.1: The 90% confidence level of (Y vs m_χ)

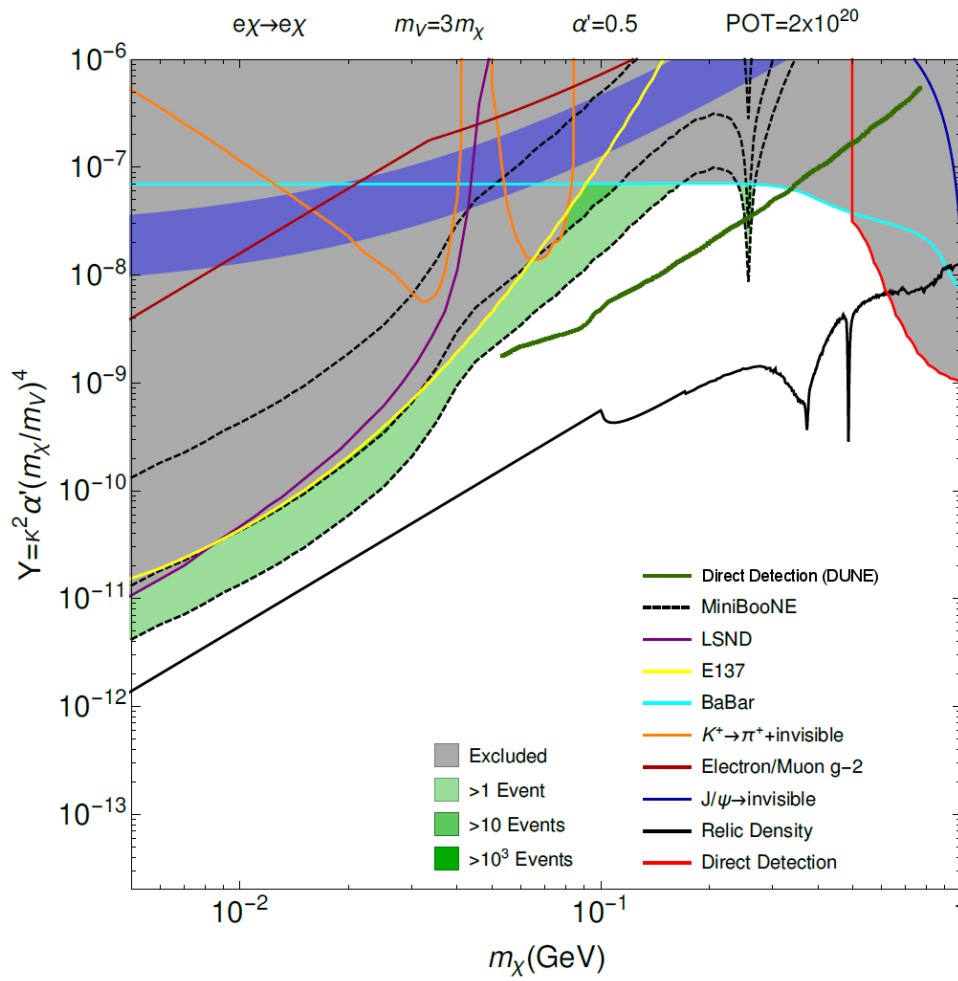


FIGURE 5.2: The 90% confidence level of (Y vs m_χ) imposed on other analyses. From Ref. [7].

Chapter 6

Conclusion

We conducted a simulated study of the light dark matter model and detection at DUNE via direct dark matter production at the target and electron scattering in the near detector. Using two constrained parameters of the light dark matter model and a range of two free parameters, a sensitivity map was shown with a 90% confidence level. Using it, we've provided knowledge of which parameter sets have the possibility of detection within the DUNE experiment. Given that a large chunk of previously unexplored parameter space is present in the sensitivity map of DUNE, it is possible that dark matter may be detected within the experiment.

There are quite a few simplifications within this analysis that may be improved upon in the future to provide a more accurate confidence level, but given this is the first project of its kind I've done, they we're necessary. One simplification is that the target material in dark matter production to a uniformly dense proton target. Many production channels of dark matter are also neglected in favor of the first order direct production channel. Theoretically, other sources of dark matter are also predicted, including π^0 decay. Same goes for the detection channels of dark matter and electron neutrinos since they are predicted to also interact with nucleons and also possibly inelastically scatter in rare cases producing a shower of secondary particles, but we chose elastic electron scattering as the detection method. Finally, the detector was greatly simplified to a rectangular fiducial volume of uniformly

dense electrons, but a realistic model of the FGT and monte carlo simulation may provide much more accurate detection results.

Appendix A

Dark Matter Job Management

Script

```

import os
import shutil
import subprocess
import sys

beam1_energy = 0.9382720813 #proton rest mass
beam2_energy = 120.0
jobcount = 250
nevents = 200000 #200000 is the max

scriptdir = os.path.abspath(sys.argv[0]+"/..")+"/"
user = os.getenv("USER")
exrootanalysis_dir = "/pnfs/dune/persistent/users/"+user+"/ExRootAnalysis.tar.gz"
gridpack_dir = "/pnfs/dune/scratch/users/"+user+"/darkmatter_gridpack/"
output_dir = "/pnfs/dune/scratch/users/"+user+"/darkmatter/"

madgraph_dir = "MG5_aMC_v2_6_1/darkphoton/"

if not os.path.exists(output_dir):
    os.makedirs(output_dir)
if not os.path.exists(scriptdir+"jobs"):
    os.makedirs(scriptdir+"jobs")
if not os.path.exists(gridpack_dir):
    os.makedirs(gridpack_dir)
if os.path.exists(output_dir+"log.log"):
    os.remove(output_dir+"log.log")

failed = []

def submit_job(vpmass, chimass, kappa, alpha):
    output_filename = "DM%lf_%lf_%lf_%lf" % (vpmass, chimass, kappa, alpha)
    script_filename = scriptdir+"jobs/"+output_filename+".sh"

    if os.path.exists(output_dir+output_filename):
        print(output_dir+output_filename+"_already_exists!")
        return
    else:
        if not os.path.exists(gridpack_dir+output_filename+"_gridpack.tar.gz"):

```

```

        script = """generate_events %s
set ebeam1 %lf
set ebeam2 %lf
set gridpack 1
set vpmass %lf
set chimass %lf
set mguser 1 %lf
set mguser 2 %lf""" % (output_file, beam1_energy, beam2_energy, vpmass, chimass, kappa, alpha)

        file_handle = open(scriptdir+"proc_card.dat", 'w')
        file_handle.write(script)
        file_handle.close()

        subprocess.call([sys.executable, '-O', madgraph_dir+"bin/madevent", scriptdir+"proc_card.dat"])

    if os.path.exists(madgraph_dir+output_file+"_gridpack.tar.gz"):
        shutil.copy2(madgraph_dir+output_file+"_gridpack.tar.gz", gridpack_dir)
    else:
        failed.append(output_file)
    return

    output = open(script_filename, "w")
    output.write("""export jobname="""+output_file+""")
source /comfs/fermilab.opensciencegrid.org/products/common/etc/setup
source /comfs/fermilab.opensciencegrid.org/products/larsoft/setup
setup ifdhc
setup python v2_7_6
setup root v6_10_04d -q e14:nu:prof

cd $_CONDOR_SCRATCH_DIR
ifdh cp """+gridpack_dir+"""+$jobname"_gridpack.tar.gz ./"$jobname"_gridpack.tar.gz
ifdh cp """+exrootanalysis_dir+"""/ExRootAnalysis.tar.gz
tar xzf "$jobname"_gridpack.tar.gz
tar xzf ExRootAnalysis.tar.gz
./run.sh """+str(nevents)+"" "$PROCESS

gzip -d events.lhe.gz
./ExRootAnalysis/ExRootLHEFConverter events.lhe unweighted_events.root

if [ -f unweighted_events.root ]; then
    echo Copying to """+output_dir+output_file+"""/"$PROCESS".root
    ifdh cp unweighted_events.root """+output_dir+output_file+"""/"$PROCESS".root
fi

echo "ALL DONE!"
""")
    output.close()
    os.chmod(script_filename, 0777)
    if not os.path.exists(output_dir+output_file):
        os.makedirs(output_dir+output_file)
    os.system("jobsub_submit.py_N_"""+str(jobcount)+""_resource=provides=usage_model=OPPORTUNISTIC_expected-lifetime_6h_OS=SL6_group=dun

#Generate scan via N-Grid
def ParametersFromNGrid():
    def step_range(smin, smax, steps):
        if steps==1:
            return [round(smin, 5)]
        else:

```

```

    size = (smax-smin)/(steps-1)
    return [round(x * size + smin, 5) for x in range(steps)]

def step_range_log(smin, smax, steps):
    if steps==1:
        return [round(smin, 5)]
    else:
        size = pow(smax/smin, 1.0/(steps-1))
        return [round(smin * pow(size, x), 5) for x in range(steps)]

# param_ranges = [
# [1],
# [0.05, 0.1, 0.15, 0.25, 0.5, 1.0, 1.5, 2.0, 2.5, 3.0, 5.0, 7.0, 10.0],
# [0.0001, 0.0005, 0.001, 0.005, 0.01],
# [0.5]
# ]

# param_ranges = [
# [1],
# [0.75, 0.2, 0.225, 0.3333, 0.7],
# [0.0002, 0.0004, 0.0008, 0.0016],
# [0.5]
# ]

param_ranges = [
[1],
[0.9, 1.3, 1.7],
[0.0015, 0.0023, 0.00338, 0.0051, 0.0076],
[0.5]
]

print("Generating_Params")
print(param_ranges)

parameter_sets = []
iteration_state = [0, 0, 0, 0]
i = 0
index = 0
while i<4:
    vpmass = param_ranges[0][iteration_state[0]]
    chimass = param_ranges[1][iteration_state[1]]
    kappa = param_ranges[2][iteration_state[2]]
    alpha = param_ranges[3][iteration_state[3]]

    # if vpmass>=chimass*3:
    #     parameter_sets.append([vpmass, chimass, kappa, alpha])

    #Constraining vpmass to chimass*3
    parameter_sets.append([chimass*3, chimass, kappa, alpha])

    index += 1
    i = 0
    while i<4:
        iteration_state[i] += 1
        if iteration_state[i]>=len(param_ranges[i]):
            iteration_state[i] = 0
            i += 1
        else:
            break

```

```

for i in parameter_sets:
    print(i[0],i[1],i[2],i[3])

raw_input("Press_Enter_to_continue...")

for i in parameter_sets:
    submit_job(i[0],i[1],i[2],i[3])

def ParametersFromFile():
    parameter_sets = []
    f = open('curve.txt')
    for line in f:
        splitted = line.split()
        chimass = float(splitted[0])
        vpmass = chimass*3
        kappa = float(splitted[1])
        alpha = 0.5
        print(vpmass, chimass, kappa, alpha)
        parameter_sets.append([vpmass, chimass, kappa, alpha])

    raw_input("Press_Enter_to_continue...")

for i in parameter_sets:
    submit_job(i[0],i[1],i[2],i[3])

#ParametersFromNGrid()
ParametersFromFile()

for fail in failed:
    print("Job_failed_to_generate:_" + fail)

```

A.1 Usage

At the beginning of the file, `beam1_energy` and `beam2_energy` specify the energy of the colliding beams. `beam1_energy` is set to the proton rest mass and `beam2_energy` is set to the DUNE proton beam energy. `jobcount` specifies the number of jobs per parameter set and `nevents` is the number of simulated events per job which cannot exceed 200,000 events. The following path declarations should be independent of the script location and the user using it, but `madgraph_dir` specifies the directory of the generated Madgraph folder for the dark matter simulation. The mode of the script is controlled by commenting/uncommenting the two function calls near the end of it. When using `ParametersFromNGrid()`, the parameter ranges are specified within that function; external file parsing for parameter ranges could be added in the future.

When using `ParametersFromFile()`, the parameters are read from 'curve.txt' in the current working directory but it is currently only configured to read m_χ and κ .

Bibliography

- [1] Edvige Corbelli and Paolo Salucci. The extended rotation curve and the dark matter halo of m33. *Monthly Notices of the Royal Astronomical Society*, 311(2):441–447, 2000. doi: 10.1046/j.1365-8711.2000.03075.x. URL <http://dx.doi.org/10.1046/j.1365-8711.2000.03075.x>.
- [2] Jenner Lynn. Hubble maps the cosmic web of ‘clumpy’ dark matter in 3-d. *NASA*, 01 2007. URL https://www.nasa.gov/mission_pages/hubble/news/clumpy_darkmatter.html.
- [3] Illustrustng media. <http://www.tng-project.org/media/>, 2017. Accessed: 2018-02-20.
- [4] J. Strait, E. McCluskey, T. Lundin, J. Willhite, T. Hamernik, V. Papadimitriou, A. Marchionni, M. J. Kim, M. Nesi, D. Montanari, and A. Heavey. Long-Baseline Neutrino Facility (LBNF) and Deep Underground Neutrino Experiment (DUNE) Conceptual Design Report Volume 3: Long-Baseline Neutrino Facility for DUNE June 24, 2015. *ArXiv e-prints*, January 2016.
- [5] R. Acciarri, M. A. Acero, M. Adamowski, C. Adams, P. Adamson, S. Adhikari, Z. Ahmad, C. H. Albright, T. Alion, E. Amador, and et al. Long-Baseline Neutrino Facility (LBNF) and Deep Underground Neutrino Experiment (DUNE) Conceptual Design Report, Volume 4 The DUNE Detectors at LBNF. *ArXiv e-prints*, January 2016.
- [6] P. deNiverville, D. McKeen, and A. Ritz. Signatures of sub-GeV dark matter beams at neutrino experiments. *Phys. Rev. D*, 86(3):035022, August 2012. doi: 10.1103/PhysRevD.86.035022.
- [7] P. deNiverville, C.-Y. Chen, M. Pospelov, and A. Ritz. Light dark matter in neutrino beams: Production modeling and scattering signatures at MiniBooNE, T2K, and SHiP. *Phys. Rev. D*, 95(3):035006, February 2017. doi: 10.1103/PhysRevD.95.035006.
- [8] F. Zwicky. On the masses of nebulae and of clusters of nebulae. *Astrophysical Journal*, 86(217):217–246, 10 1937. URL <http://adsabs.harvard.edu/doi/10.1086/143864>.
- [9] Vera C. Rubin and W. Kent Jr. Ford. Rotation of the andromeda nebula from a spectroscopic survey of emission regions. *Astrophysical Journal*, 159(379):379–408, 02 1970. URL <http://adsabs.harvard.edu/doi/10.1086/150317>.

- [10] S. Boran, S. Desai, E. Kahya, and R. Woodard. GW170817 Falsifies Dark Matter Emulators. *ArXiv e-prints*, October 2017.
- [11] Julia Keller. Modeling the universe. *MIT News*, 01 2018. URL <http://news.mit.edu/2018/modeling-universe-Vogelsberger-IllustrisTNG-0131>.
- [12] R. Acciarri, M. A. Acero, M. Adamowski, C. Adams, P. Adamson, S. Adhikari, Z. Ahmad, C. H. Albright, T. Alion, E. Amador, and et al. Long-Baseline Neutrino Facility (LBNF) and Deep Underground Neutrino Experiment (DUNE) Conceptual Design Report Volume 1: The LBNF and DUNE Projects. *ArXiv e-prints*, January 2016.
- [13] B. A. Dobrescu and C. Frugiuuele. GeV-scale dark matter: production at the Main Injector. *Journal of High Energy Physics*, 2:19, February 2015. doi: 10.1007/JHEP02(2015)019.
- [14] B. Batell, P. deNiverville, D. McKeen, M. Pospelov, and A. Ritz. Lepophobic dark matter at neutrino factories. *Phys. Rev. D*, 90(11):115014, December 2014. doi: 10.1103/PhysRevD.90.115014.
- [15] C. D. Carone and H. Murayama. Possible Light U(1) Gauge Boson Coupled to Baryon Number. *Physical Review Letters*, 74:3122–3125, April 1995. doi: 10.1103/PhysRevLett.74.3122.
- [16] C. D. Carone and H. Murayama. Realistic models with a light U(1) gauge boson coupled to baryon number. *Phys. Rev. D*, 52:484–493, July 1995. doi: 10.1103/PhysRevD.52.484.
- [17] B. Batell, M. Pospelov, and A. Ritz. Exploring portals to a hidden sector through fixed targets. *Phys. Rev. D*, 80(9):095024, November 2009. doi: 10.1103/PhysRevD.80.095024.
- [18] M. Pospelov, A. Ritz, and M. Voloshin. Secluded WIMP dark matter. *Physics Letters B*, 662:53–61, April 2008. doi: 10.1016/j.physletb.2008.02.052.
- [19] E. Izaguirre, G. Krnjaic, P. Schuster, and N. Toro. Analyzing the Discovery Potential for Light Dark Matter. *Physical Review Letters*, 115(25):251301, December 2015. doi: 10.1103/PhysRevLett.115.251301.
- [20] Pavel M. Nadolsky, Hung-Liang Lai, Qing-Hong Cao, Joey Huston, Jon Pumplin, Daniel Stump, Wu-Ki Tung, and C.-P. Yuan. Implications of cteq global analysis for collider observables. *Phys. Rev. D*, 78:013004, Jul 2008. doi: 10.1103/PhysRevD.78.013004. URL <https://link.aps.org/doi/10.1103/PhysRevD.78.013004>.
- [21] Fermilab computing. <http://www.fnal.gov/pub/science/computing/grid.html>, 2015. Accessed: 2018-03-06.

- [22] J. Alwall, R. Frederix, S. Frixione, V. Hirschi, F. Maltoni, O. Mattelaer, H.-S. Shao, T. Stelzer, P. Torrielli, and M. Zaro. The automated computation of tree-level and next-to-leading order differential cross sections, and their matching to parton shower simulations. *Journal of High Energy Physics*, 7:79, July 2014. doi: 10.1007/JHEP07(2014)079.
- [23] Amy Williams, Steve Barrus, R. Keith Morley, and Peter Shirley. An efficient and robust ray-box intersection algorithm. *Journal of Graphics Tools*, 10(1):49–54, 2005. doi: 10.1080/2151237X.2005.10129188. URL <https://doi.org/10.1080/2151237X.2005.10129188>.
- [24] T. Alion, J. J. Back, A. Bashyal, M. Bass, M. Bishai, D. Cherdack, M. Diwan, Z. Djurcic, J. Evans, E. Fernandez-Martinez, L. Fields, B. Fleming, R. Gran, R. Guenette, J. Hewes, M. Hogan, J. Hylen, T. Junk, S. Kohn, P. LeBrun, B. Lundberg, A. Marchionni, C. Morris, V. Papadimitriou, R. Rameika, R. Rucinski, S. Soldner-Rembold, M. Sorel, J. Urheim, B. Viren, L. Whitehead, R. Wilson, E. Worcester, and G. Zeller. Experiment Simulation Configurations Used in DUNE CDR. *ArXiv e-prints*, June 2016.
- [25] R. Gandhi, P. Ghoshal, S. Goswami, P. Mehta, S. Uma Sankar, and S. Shalgar. Mass hierarchy determination via future atmospheric neutrino detectors. *Phys. Rev. D*, 76(7):073012, October 2007. doi: 10.1103/PhysRevD.76.073012.